frontiers in Earth Science

ORIGINAL RESEARCH
published: 12 February 2021
doi: 10.3389/feart.2020.521766

Stratigraphic Architecture of the Karoo River Channels at the End-Capitanian

Emese M. Bordy and Francisco Paiva*

Department of Geological Sciences, University of Cape Town, Cape Town, South Africa

The main Karoo Basin of southern Africa contains the continental record of the end-Triassic, end-Permian, and end-Capitanian mass extinction events. Of these, the environmental drivers of the end-Capitanian are least known. Integrating quantitative stratigraphic architecture analysis from abundant outcrop profiles, paleocurrent measurements, and petrography, this study investigates the stratigraphic interval that records the end-Capitanian extinction event in the southwestern and southern main Karoo Basin and demonstrates that this biotic change coincided with a subtle variation in the stratigraphic architectural style ~260 Ma ago. Our multi-proxy sedimentological work not only defines the depositional setting of the succession as a megafan system that drained the foothills of the Cape Fold Belt, but also attempts to differentiate the tectonic and climatic controls on the fluvial architecture of this paleontologically important Permian succession. Our results reveal limited changes in sediment sources, paleocurrents, sandstone body geometries, and possibly a constant hot, semi-arid paleoclimate during the deposition of the studied interval; however, the stratigraphic trends show upward increase in 1) laterally accreted, sandy architectural elements and 2) architectural elements that build a portion of the floodplain deposits. We consider this to reflect a long-term retrogradational stacking pattern of facies composition that can be linked to changes on the medial parts of southward draining megafans, where channel sinuosity increased, and depositional energy decreased at the end-Capitanian. The shift in the fluvial architecture was likely triggered by basin-wide allogenic controls rather than local autogenic processes because this trend is observed in the coeval stratigraphic intervals from geographically disparate areas in the southwestern and southern main Karoo Basin. Consequently, we propose that this regional backstepping most likely resulted from tectonic events in the adjacent Cape Fold Belt.

Keywords: Permian megafans, tectonic control, main Karoo Basin, paleocurrent patterns, end-Capitanian, fluvial facies architecture, quantitative stratigraphy

OPEN ACCESS

Edited by:
Ivar Midtkandal,
University of Oslo, Norway

Reviewed by:
Amanda Owen,
University of Glasgow, United Kingdom
Luca Colombera,
University of Leeds, United Kingdom

****Correspondence:***
Emese M. Bordy
emese.bordy@uct.ac.za

Specialty section:
This article was submitted to Sedimentology, Stratigraphy and Diagenesis, a section of the journal Frontiers in Earth Science.

Received: *19 December 2019*
Accepted: *15 December 2020*
Published: *12 February 2021*

Citation:
Bordy EM and Paiva F (2021) Stratigraphic Architecture of the Karoo River Channels at the End-Capitanian. Front. Earth Sci. 8:521766. doi: 10.3389/feart.2020.521766

Abbreviations:: MKB, main Karoo Basin; CFB, Cape Fold Belt; Myr, millions of years; AE, architectural element*; AT, architecture type*; CB, channel belt; FU, floodplain unit; CC, channel-belt complex; CCS, channel-belt complex sets; W, width; T, thickness; S, W, E, N, NE, NW, etc., south, west, east, north, north-east, etc. cardinal directions. *For lithofacies codes, see Table 2; for architectural element codes, see Table 1; for architecture types, see Table 3.

INTRODUCTION

Tectonics and climate, the two main allogenic forcing mechanisms of continental deposition (Shanley and McCabe, 1994; Allen et al., 2002; Catuneanu, 2006), are fundamentally associated with the history and evolution of the Lower Beaufort Group in the main Karoo Basin (MKB) of South Africa (**Figure 1**). The overall tectonic and climatic settings of the basin in the Permian are thought to be fairly well understood (Keyser and Smith, 1978; Smith, 1979, Smith 1987; Catuneanu et al., 1998, Catuneanu and Bowker, 2001; Cole and Wipplinger, 2001; Catuneanu et al. 2005; Bordy et al., 2011). However, the intertwined impact of the two mechanisms on the Karoo sedimentation patterns is often difficult to determine at time scales $< 10^6$ years. In the Permian Lower Beaufort Group (**Figure 1C**), a succession of ~16.5 Myr in duration and >2,500 m in thickness, the subtle spatiotemporal changes in the fluvio-lacustrine sedimentary and volcaniclastic processes have made detailed lithostratigraphic subdivisions and correlations problematic. This resulted in a proliferation of informal and often discordant lithostratigraphic nomenclatures, which use sand-to-mud ratio and vertebrate fossil content as a proxy for defining formations (for summaries, see Cole and Wipplinger, 2001; Day and Rubidge, 2014; Day et al., 2015; Cole et al., 2016; Day and Rubidge, 2020).

Using quantitative stratigraphic architecture analysis, including paleocurrent and petrographical data collected from a regional outcrop network, this study aims to untangle the climatic, tectonic, and other, more intrinsic syn-sedimentary signals of a ~260 Ma old rock record in the southwestern and southern MKB (**Figure 1**). The significance of this stratigraphic interval, which is conformable, and span ~2.0–2.5 Myr in total duration and ~600 m in thickness (**Figure 1C** and references in there), is that it contains evidence not only for fluvial architectural changes, but also for a rich and diverse paleontological record associated with the end-Capitanian mass extinction event (Day et al., 2015), also known as the "dinocephalian extinction event" of Lucas (2017). In this quantitative facies analysis study, we aim to 1) demonstrate that the depositional setting for this ~260 Ma old paleontologically important Permian succession was a spatiotemporally dynamic megafan system that drained the foothills of the adjacent Cape Fold Belt (CFB) and 2) differentiate the tectonic and climatic controls on the changing fluvial architecture, while emphasizing the limitations of the fluvial sedimentary record for capturing megaevents, which are sudden, high magnitude environmental perturbations that may have caused mass extinction events.

GEOLOGICAL BACKGROUND

Karoo Stratigraphy

Covering an area of ~600,000 km^2 in South Africa and all of Lesotho (**Figure 1**), the main Karoo Basin is the largest sedimentary depocenter that formed in southwestern Gondwana from the Late Paleozoic to Middle Mesozoic (Johnson et al., 1996; 2006). The basin is notable for containing a succession, formally named the Karoo Supergroup, which represents a geological history of ~120 Myr in duration (**Figure 1**–Johnson et al., 1996; Rubidge, 2005). The Karoo Supergroup, being the most widespread stratigraphic unit in southern Africa, fills the similar aged basins to the MKB that are spread across the region and all the way to the Sahara Desert in the north (Catuneanu et al., 1998; Catuneanu et al., 2005). The Karoo Supergroup preserves the record of major geological and biotic events that range from the formation of Permo-Carboniferous glacial deposits to the extrusion and intrusion of Lower Jurassic igneous complexes as well as several mass extinction events (e.g., end-Capitanian, end-Permian, and end-Triassic: Johnson et al., 1996; Rubidge, 2005; Rubidge et al., 2013; Day et al., 2015).

The Beaufort Group, which is the Middle Permian to Middle Triassic part of the Karoo Supergroup, represents the first continental fluvial and lacustrine strata in the MKB. The succession is >2500 m thick and consists of mainly mudstones and sandstones, which preserve an outstandingly rich and fairly diverse vertebrate fossil heritage that is dominated by pre-mammalian land-dwelling tetrapods (Keyser and Smith, 1978; Hancox and Rubidge, 2001; Rubidge, 2005). This abundant therapsid fossil fauna not only allowed the biostratigraphic subdivision of the Beaufort Group into eight vertebrate assemblage zones (**Figure 1C**), but also turned the unit into a global biostratigraphic standard for the Middle Permian to Early Triassic continental vertebrates (Rubidge, 2005; Viglietti et al., 2016; Day and Rubidge, 2020). The stratigraphic interval studied here (**Figure 1C**) is from the Lower Beaufort Group and straddles the uppermost part of the Abrahamskraal and the lowermost Teekloof Formations in two regions of the southwestern and southern MKB (abbreviated here as SW-MKB and S-MKB, respectively, and further subdivided into W1, W2, and E study sectors–**Figure 1**). The studied succession (**Figure 1C**) was described from the SW-MKB in sedimentological (Stear, 1978, Stear, 1980, Stear, 1983, Stear, 1985; Smith, 1987, Smith, 1990; Gulliford et al., 2014; Wilson et al., 2014), biostratigraphic, and taphonomic studies (Keyser and Smith, 1978; Loock et al., 1994; Smith, 1979, Smith, 1993). These studies have established that the deposition of this Permian succession occurred in a fluvio-lacustrine setting under a semi-arid climate.

Tectonic Setting of the Main Karoo Basin

The generation and evolution of the MKB, according to a retro-arc foreland basin model (Catuneanu et al., 1998), are generally accepted. The model explains the stratigraphic relationships in the Karoo Supergroup as primarily resulting from the flexural behavior of the lithospheric plate in southern Gondwanan from the Late Carboniferous to the Early Jurassic. The flexural behavior is thought to have been controlled by subduction of the paleo-Pacific Plate under the southern margin of Gondwana in a compressional tectonic setting. Simultaneously, mountain building resulted in the CFB as the orogen adjoining the MKB in the south (**Figure 1**). Multiple episodes of supracrustal loading and unloading events during the Cape Orogeny directly influenced the spatiotemporal evolution of the flexural tectonic provinces in the basin and resulted in repeated movement of the

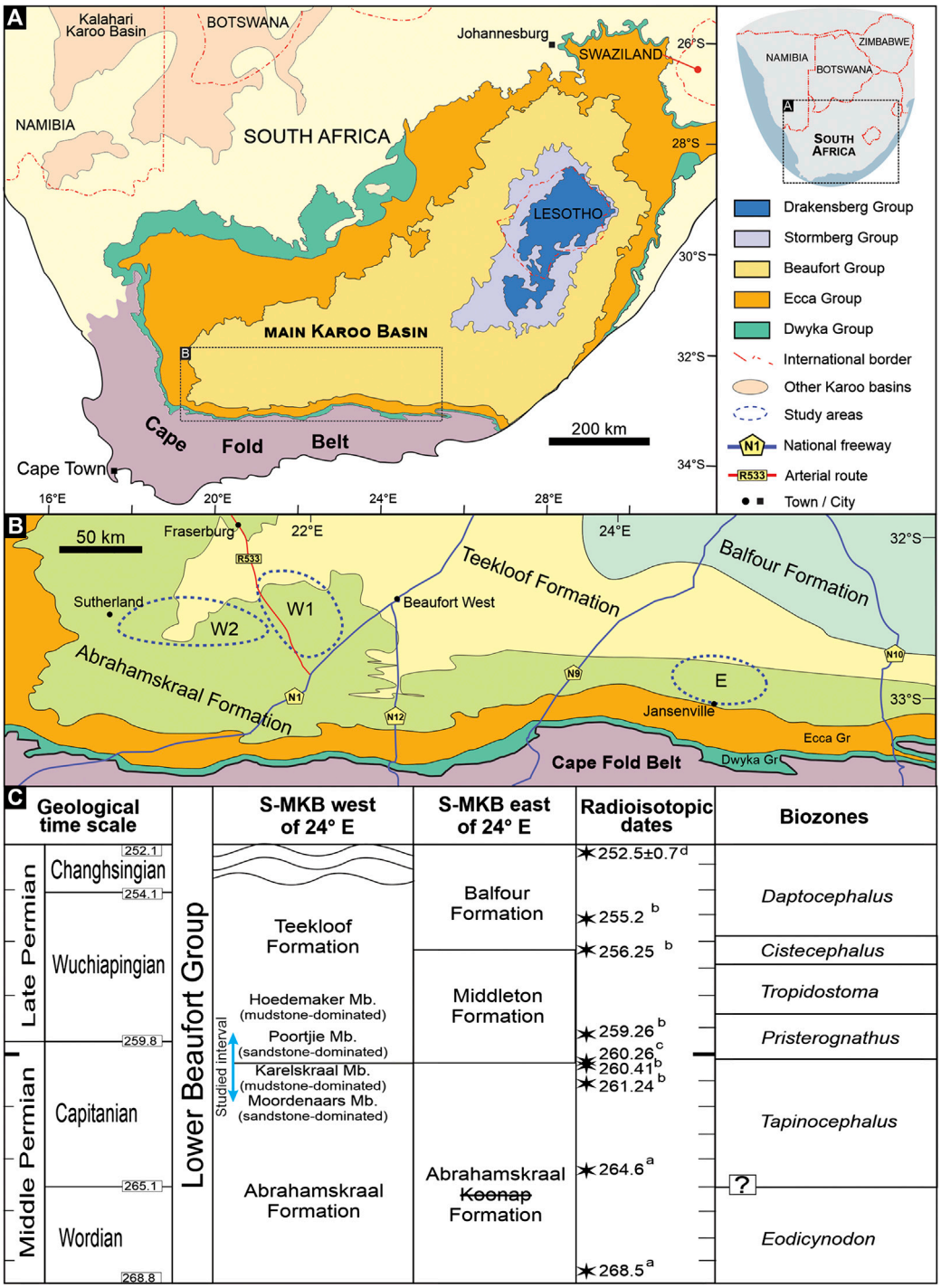

FIGURE 1 | Locality map and stratigraphy of the study region in the southwestern main Karoo Basin (MKB) in South Africa. **(A)** Simplified geological map of the MKB and other Karoo Basins of southern Africa. The spatial distribution of the main stratigraphic units of the Karoo Supergroup is only shown for the MKB. **(B)** The study areas are within the Lower Beaufort Group and straddle the boundary of the Abrahamskraal and Teekloof/Middleton Formations (see circles with dashed lines marking the study areas cross the solid line marking the formation boundary). Abbreviations of the study areas: W1: eastern sector and W2: western sector in the SW-MKB; E: S-MKB. Geological map modified from Johnson and Wolmarans (2008). **(C)** The litho- and biostratigraphy of the Lower Beaufort Group in the southwestern and southern main Karoo Basin. Modified after Rubidge (2005), Rubidge et al. (2013), Day et al. (2015), Viglietti et al. (2016). Numerical ages are listed in Ma. Radioisotopic dates are from a: Lanci et al. (2013); b: Rubidge et al. (2013); c: Day et al. (2015); d: Coney et al. (2007). The Koonap Formation was renamed to Abrahamskraal Formation (Cole et al., 2016). Note the different nomenclature (Teekloof and Middleton formations) used for the two lithostratigraphically equivalent units in the Lower Beaufort Group (herein referred to as the Teekloof Formation for simplicity). The arenaceous units (named Moordernaars and Poortjie Members in western study area) are the focus of this study. Wavy lines indicate post-Karoo erosion.

TABLE 1 | Description and interpretation of the architectural elements from the studied stratigraphic interval in the southwestern and southern main Karoo Basin. Modified after Miall (1985); Miall (1996), Long (2006), and Colombera et al. (2013). See **Table 2** for facies descriptions.

Architectural element (AE)	Description			Interpretation
	Geometry	Facies combinations	Other characteristics	
CH–aggradational channel fill	Finger, lens, or sheet	Any combination, but mostly sandy and gravelly facies	Vertically stacked depositional increments dominated by horizontal internal bounding surfaces. Downstream-elongated, concave-up erosional base	Infill of channel belts primarily by aggradation
LA–lateral accretion barform	Wedge, sheet, lobe	St, Sp, Sh, Sl, Sr1, Sr2, Gmm1, Gmm2, Gcm, Gch	Laterally stacked units at high/right angle to the paleoflow. Sharp, sub-horizontal to slightly concave-up internal bounding surfaces and often erosional base	Infill of channel belts by laterally migrating bars (e.g., point bars)
DA–downstream accretion barform	Lens	St, Sp, Sh, Sl, Sr1, Sr2, Gmm1, Gmm2, Gcm, Gch	Downstream stacked units at low angle to the paleoflow. Downstream-dipping low angle (<10°) internal bounding surfaces. Sub-horizontal to slightly concave-up and often erosional bases	Infill of channel belts by downstream migrating bars
DLA–downstream and lateral accretion barform	Wedge, lens	St, Sp, Sh, Sl, Sr1, Sr2, Gmm1, Gmm2, Gcm, Gch	Intermediate bar form between LAs and DAs; dominated by oblique accretions relative to the main paleoflow, with a combination of downstream accretions on the downstream ends and lateral accretion along the flanks. Vertical accretion is volumetrically minor	Infill of channel belts by the migration of bars that accrete both downstream and laterally in comparable proportions
GB–gravel barform	Lens, ribbon	Gmm1, Gmm2 > Gch	Coarse-grained units (with gravel size clasts) that commonly overlie an irregular erosional base. Beds are 0.4–1 m thick and 1 m–~15 m wide. Often fine upwards and downwards	Deposits from peak flow in high energy events, in-channel migrating dunes, or gravel bars
SG–sediment Gravity-flow	Lobe, ribbon, sheet	Sm, Gmm1, Gmm2	Irregular, sharp but often non-erosional base. Internally often structureless; interbedded with GB	Mass movement (hyperconcentrated flows/ mass flows) deposits from waning-flow in floods or bank collapse
AC–abandoned channel fill	Lens, ribbon	As in CH but contains a higher proportion of fine-grained facies in its upper part	Channelized, heterolithic unit dominated by vertically stacked facies; always fines upwards	Channel abandonment leading to ponding of waters and suspension settling of mud-size particles with or without organic components
LV–levee	Wedge	Fl, Sh, Sr	Heterolithic unit that tapers and fines away from the channel margin; poorly defined base and low-angle, internal surfaces that can offlap or downlap; grades laterally into mainly FF. Paleoflow is usually at high angles to that in the main channel	Aggradational deposits in areas separating channels from the floodplain; i.e., the most proximal overbank deposits next to channel margins
CR–crevasse channel	Lens, ribbon	St, Sm, Sh, Sl, Sr, Fm	Channelized, sandy unit with concave-up, erosional base. Paleoflow is usually at high angles to that in the main channel. Always associated with other floodplain AEs (i.e., LV, CS, FF)	Infill of subordinate channels; link main channel to adjacent floodplain by tapping into main channel and feeding crevasse splays during floods
CS–crevasse splay	Tongue-shaped, flat wedge	St, Sm, Sl, Sr, Fl, Fm	Sandy unit with low-angle downlapping internal accretion surfaces. Thins and fines away from channel margin, and interfingers or grades laterally into mainly FF. Sharp, slightly erosive base. Paleoflow is usually at high angles to that in the main channel. Laterally more extensive than LV	Progradational to aggradational deposits that form in overbank settings as crevasse splays near main channels due to periodic unconfined flow emerging from crevasse channels (or the main channel)
SB–sandy bedforms	Tabular, lenticular	Sh, Sl, Sm > Sr1, Sr2	Thin to thick, vertically stacked, laterally persistent, sandstone-dominated unit with sharp, planar to irregular lower bounding surfaces that can be slightly erosive (non-channelized)	Aggradational deposits from fast traction-currents in repeated unconfined, sheet-like flows on the floodplain (?terminal splays in overbank area)
FF–overbank fines	Tabular	Fm, Fl >> Sr, Sm	Thin to thick, vertically stacked, laterally persistent, mudstone-dominated unit; pedogenic alteration features are common	Aggradational deposits from suspension settling (or as bedload deposition of mud aggregates) in unconfined flows on the floodplain

TABLE 2 | Fluvial lithofacies descriptions and interpretations (modified after Miall, 1985, Miall, 1996) from the studied stratigraphic interval in the southwestern and southern main Karoo Basin. Abbreviations: W1: eastern sector and W2: western sector in the southwestern main Karoo Basin; E: southern main Karoo Basin. Also see **Figure 3** for field photographs of the lithofacies, **Figure 1** for the relative positions of W1, W2, and E, and **Supplementary Material** for the more detailed descriptions of the facies in the different study sectors.

Facies code	Description	Interpretation	Abrahamskraal Formation			Teekloof Formation		
			W1	W2	E	W1	W2	E
Gmm1	Gravel, matrix-supported, massive breccia. Clasts (av. 5 cm) are sandstones granule/pebbles, intraformational mudstones, carbonate concretions. Weak grading. Mostly found at the base of channels (i.e., basal gravel)	Forms from plastic debris flow during bank collapse, due to renewed channel flow strength. Lack of structures means rapid flow speed reduction and/or rapid decrease in sediment overload	✓	✓	✓		✓	✓
Gmm2	Gravel, matrix-supported, massive breccia (clast-rich sandstone). Clasts (av. 9 cm) are mostly rip-up mudstones chips (intraformational). Carbonate concretions and sandstone pebbles are common. Weak to normal grading. Mostly found in the middle of channel sequences	Forms from plastic debris flow during bank collapse, due to renewed channel flow strength. Lack of structures means rapid flow speed reduction and/or rapid decrease in sediment overload	✓	✓	✓		✓	✓
Gcm	Gravel, clast-supported, massive conglomerates. Clasts (av. 10 cm) are mainly granules/pebble-size sandstone, carbonate concretions, rare mudstone, and fossilized wood fragments. Weak grading	As in Gmm1. Roundness of mineralogically and texturally stable clasts may indicate long travel distances or high energy grinding action		✓	✓		✓	✓
Gch	Gravel, clast-supported, horizontal bedded conglomerate. Clasts (av. 5 cm) are sandstones granules/pebbles, mudstones, concretions, and fossilized wood. Weak grading. Mostly found at the base of channel deposit successions (i.e., basal gravel)	Forms as longitudinal bedforms in open channels. Possibly produced during lower frequency, high magnitude discharge events. Horizontal bedding indicates sustained flow	✓		✓			✓
Sm	Sand, mostly fine-grained, occasionally medium- and rarely coarse-grained, massive	Forms due to mass movements (hyperconcentrated flows/mass flows) from waning-flow in floods or bank collapse. Alternatively, primary structures destroyed by bioturbation, dewatering, or weathering (recent)	✓	✓	✓	✓	✓	✓
Sh	Sand, mostly fine-grained, occasionally medium- and rarely coarse-grained. Horizontal lamination	Forms as plane bedforms in upper flow conditions in shallow water depths	✓	✓	✓	✓	✓	✓
Sl	Sand, mostly fine-grained, occasionally medium-grained. Low-angle cross-bedding (foreset dip angle <10°)	Forms as large-scale dunes and barforms, scour fills, humpback or washed-out dunes, antidunes	✓	✓	✓	✓	✓	✓
St	Sand, mostly fine-grained, occasionally medium- and rarely coarse-grained. Trough cross-bedding	Forms from the migration of 3D sinuous-crested dunes in higher flow regimes than Sp	✓	✓	✓	✓	✓	✓
Sp	Sand, mostly fine-grained, occasionally medium- and rarely coarse-grained. Planar cross-bedding. Common at the base of channel belts	Forms from the migration of 2D straight-crested dunes (transverse bedforms)	✓	✓	✓	✓	✓	✓
Sr1	Sand, very fine- to fine-grained. Climbing ripple cross-lamination	Forms from the migration of ripples in a low flow regime. Sr can form on levees, in crevasse channels, and on point bars during waning phases of flow	✓	✓	✓	✓	✓	✓
Sr2	Sand, very fine- to fine-grained. Wavy or trough ripple cross-lamination (flasers)	Forms from the migration of ripples in a low flow regime. Mud drapes define the troughs and they form when currents periodically stop allowing mud to settle from suspension			✓			
Ss	Sand, fine-grained to very coarse-grained, may be pebbly, broad shallow scours. Normal grading	Forms as scour-structures are filled up during the waning phase of floods. Grades into mudstone	✓	✓	✓	✓	✓	✓
Sb	Sand, very fine-grained, often fine- grained, and occasionally medium-grained. Ball-and-pillow structures and convolute laminations	Forms as pore water moves/escapes from and disrupts the previously settled, soft sediment (due to fast rates of sedimentation). Soft sediment deformation	✓	✓	✓	✓	✓	✓
Fl1	Fines, silt size, laminated, purple-red color	Forms from suspension settling in waning flood in overbank or abandoned channels. Purple-red color may indicate subaerial and oxidizing conditions shortly after deposition	✓	✓	✓	✓	✓	✓
Fl2	Fines, silt size, laminated, olive green-grey color	Forms from suspension settling in waning flood in overbank or abandoned channels. Green-grey color may indicate subaqueous and reducing conditions shortly after deposition	✓	✓	✓	✓	✓	✓
Fsm1	Fines, silt size, weakly laminated to massive, purple-red color, blocky weathering	As in Fl1. Absence of laminations may indicate either quick deposition (e.g., mudflows) or bioturbation	✓	✓	✓	✓	✓	✓
Fsm2	Fines, silt size, massive, olive green-grey color, blocky weathering	As in Fl2. Absence of laminations may indicate either quick deposition (e.g., mudflows) or bioturbation	✓	✓	✓	✓	✓	✓
Fb	Fines, silt size, ball-and-pillow structures, and convolute bedding	As in Sb	✓	✓	✓	✓	✓	✓

(Continued on following page)

TABLE 2 | (*Continued*) Fluvial lithofacies descriptions and interpretations (modified after Miall, 1985, Miall, 1996) from the studied stratigraphic interval in the southwestern and southern main Karoo Basin. Abbreviations: W1: eastern sector and W2: western sector in the southwestern main Karoo Basin; E: southern main Karoo Basin. Also see Figure 3 for field photographs of the lithofacies, Figure 1 for the relative positions of W1, W2, and E, and Supplementary Material for the more detailed descriptions of the facies in the different study sectors.

Facies code	Description	Interpretation	Abrahamskraal Formation			Teekloof Formation		
			W1	W2	E	W1	W2	E
Fmd	Fines, silt size, massive with desiccation cracks	Forms from suspension settling in waning flood in overbank or abandoned channels, and subsequent subaerial exposure causing mud-drapes/layers to crack. Indicates localized low deposition rates	✓	✓	✓	✓	✓	✓
Fr	Fines, silt size, massive, roots, bioturbation, mottling texture of colors (green-grey and purple-red)	Forms from suspension settling in waning flood in overbank or abandoned channels, and subsequent bioturbation by mainly rootlets (affecting the reducing/oxidizing reactions in the sediment)		✓	✓	✓	✓	✓
T	Very fine-grained, often cherty layers	Forms via the consolidation of subaerial volcanic ash (tuff)			✓			
P	Paleosol with carbonate concretions, rootlets, etc.	Ancient soil with *in situ* carbonate precipitation	✓	✓	✓	✓	✓	✓

depocenter through time from S to N and vice versa. During the Permian, the southern MKB, in which the fluvio-lacustrine Lower Beaufort Group accumulated, was a foredeep depression with a subsidence rate primarily driven by the orogenic events of the adjacent CFB (Catuneanu et al., 1998).

An alternative hypothesis by Tankard et al. (2012) proposes a basin evolution model in which the MKB was initiated by rigid basement block movement associated with crustal faults and lithospheric deflection due to subduction-driven mantle flow. In this model, the Permian fluvial succession was deposited in a "ramp syncline" where subsidence was due to mantle extension and vertical displacement along crustal-scale extensional faults episodically uplifted the southern basin-margin. This model suggests that the Cape Orogeny only started playing a role in the evolution of the MKB close to the Permian-Triassic boundary. Recent geochronological constraints disagree on the evolution of the Cape Orogeny with regards to the number, timing, and onset of the of Cape deformation events. For example, high-precision $^{40}Ar/^{39}Ar$ step-heating analyses by Blewett and Phillips (2016) and Blewett et al. (2019) constrained one major phase of CFB deformation that occurred between 253.4 and 249.6 Ma, although "earlier episodic or prolonged deformation events cannot be excluded" (Blewett et al., 2019, p. 219). While the 253.4–249.6 Ma range is interpreted as either the peak or he final dominant phase of CFB deformation, Hansma et al. (2015) demonstrated, using a more robust dataset, that in addition to the Permo-Triassic deformation event, the onset of deformation was some 20–25 Myr earlier, around 275 Ma (Kungurian) and that, on large scale, the orogenic front propagated northward in a time-transgressive manner throughout the evolution of the basin. In summary, while our study is not meant to contest whether the MKB was initiated due to flexural deflection and/or crustal faulting, we cannot ignore the geochronological message from the CFB suggesting that indeed the CFB could have been emergent (as part of the larger Gondwanide Orogen) and acted as a sediment source for the MKB already in the Paleozoic. This is fundamental for reaching a reliable interpretation of the sediment composition, paleocurrents, and overall sedimentation dynamics in the MKB during the investigated end-Capitanian interval.

METHODS

This research is a qualitative and quantitative assessment of the fluvial facies architecture across the contact of the Abrahamskraal and Teekloof Formations, which is currently presumed to capture the terrestrial end-Capitanian Mass Extinction Event ~260 Ma ago. The extent of the overall study region is ~500 km in length (**Figures 1A**,**B**). The GPS coordinates of the thirty-five study sites are in **Supplementary Table S1** and their spatial projection in Bordy (2018). In the SW-MKB, two adjacent study areas were investigated (W1, W2 in **Figure 1**); here the studied stratigraphic interval is a ~600 m thick sedimentary succession extending from the upper Abrahamskraal Formation into the Poortjie Member of the lower Teekloof Formation (**Figure 1C**). In the S-MKB, the same stratigraphic interval was studied in a ~400 m thick succession. Here, vegetation cover is higher, and good exposures are mainly found in incised river/stream valleys and on hill slopes rather than in road cuttings.

In this study, we used the mature, standard method of fluvial lithofacies classification and analysis based on works by Miall (1985), Miall (1988), Miall (1996), Gibling (2006), and Colombera et al. (2013). The lithofacies types in this study were assessed qualitatively in the field and are presented in **the Results**. Abundant, high-quality, 3D exposures at thirty-five study sites allowed the generation of the outcrop lithofacies maps (see **Supplementary Table S1**, for the full list of study sites and coordinates). In each outcrop, in order to map the spatial distribution of the lithofacies and outline the key sedimentological surfaces, we draw outcrop sketches, took photographs, and measured representative centimeter-scale sedimentary facies logs. To turn a given exposure into a digital outcrop lithofacies map, we took overlapping field photographs perpendicular to the outcrop, digitally merged them into photopanels (see Wizevich, 1992), and traced them over with

the aid of our field sketches and graphical software packages. Using a typical outcrop from the Abrahamskraal Formation in the western study area, this lithofacies mapping process is illustrated in **Supplementary Figure S1**, which shows how the integration of two outcrop images perpendicular to each other (**Supplementary Figures S1A, S1B**) and a representative centimeter-scale sedimentary facies log (**Supplementary Figure S1C**) give a 3D control over the facies distributions (and that of the AEs, see below).

To reconstruct the origin of the sedimentary rocks in the studied stratigraphic interval, we 1) measured paleocurrent indicators (e.g., parting lineation, trough- and planar cross-bedding; High and Picard, 1974; Miall, 1974; Dasgupta, 2002) and 2) analyzed the petrography (i.e., texture and composition) of twenty-three sandstone samples using the Gazzi-Dickinson point-counting method (Dickinson, 1970, Dickinson, 1985; Ingersoll et al., 1984). In addition to paleo-drainage analysis, the paleocurrent measurements are also important for differentiating between various fluvial architectural elements (see **Table 1**). A concerted effort was made to obtain as many paleocurrent measurements as possible (see Miall, 2016, p. 299). To limit the bias of grain size over the composition of the sandstone samples, we only sampled fine-grained sandstones from locations listed in **Supplementary Table S1**. For the classification of the sandstones, we used the descriptive petrographic classification scheme proposed by Garzanti (2016, 2019).

The central concept of this study of fluvial facies architecture is that the complex and heterogeneous rock record of fluvial systems is made up of units that are repeated, hierarchical, and predictable, and therefore, their systematic study will likely result in an effective understanding of their genesis (Allen, 1983; Miall, 1985; Miall, 1988; Leeder, 1993; Miall, 1996; Gibling, 2006; Payenberg et al., 2011; Colombera et al., 2013; Miall, 2013; Gulliford et al., 2014; Wilson et al., 2014; Miall, 2016; Owen et al., 2017a). While there are several different schemes/terminologies in the literature (Miall 1996, figure 4.2; Colombera et al., 2013, figure 1; Hampson et al., 2013, figure 5; Gulliford et al., 2014, figure 5; Owen et al., 2017a, figure 1), our summary on how the different fluvial sedimentary building units and their hierarchy may be identified in the outcrop lithofacies maps on scales ranging from 1 to 100s of meters is schematically shown in **Figure 2**. This scheme is based on a similar one developed specifically using the Lower Beaufort Group as a case study by Gulliford et al. (2014) (see their figure 5 for comparison).

In the hierarchy of fluvial architecture systems, the lithofacies are the basic building blocks and describe the physical and biological properties of rocks at centimeter to decimeter scale. How this level of the hierarchy builds the next level is not shown in **Figure 2**, but this has been illustrated in the earlier works (e.g., Miall 1996, figure 4.13; Colombera et al., 2013, figure 1; Gulliford et al., 2014, figure 5; Owen et al., 2017a, figure 1). Moreover, the genetic relationship between fluvial lithofacies or lithofacies groups (i.e., architectural elements–see below) and depositional landscape features (e.g., bedforms, macroforms) is not discussed here but is the subject of past research (e.g., Leeder, 1993; Miall 1996, table 4.2; Hampson et al., 2013, figure 5; Miall, 2016, figure 9; Owen et al., 2017a, figure 1). The description and interpretation of the basic building blocks in our study area are presented in **the Results**.

The groups of lithofacies that are three-dimensionally recurring form lithofacies associations with distinctive 3D geometry and are termed architectural elements (AEs). From this definition follows that the various AEs are depositional units with decimeter to a few meter thickness that can be differentiated from each other by the lithofacies associations (groups) and the internal spatial arrangement of the lithofacies within the individual AEs. The latter (i.e., the accretion geometries of the lithofacies) can be interpreted in terms of fluvial morphodynamics and are therefore indicative of subenvironment of deposition. Two examples of standard, sandstone-dominated AEs (i.e., LA: lateral accretion barform and DA: downstream accretion barform) are schematically shown to be encased in mudstone-dominated, "overbank

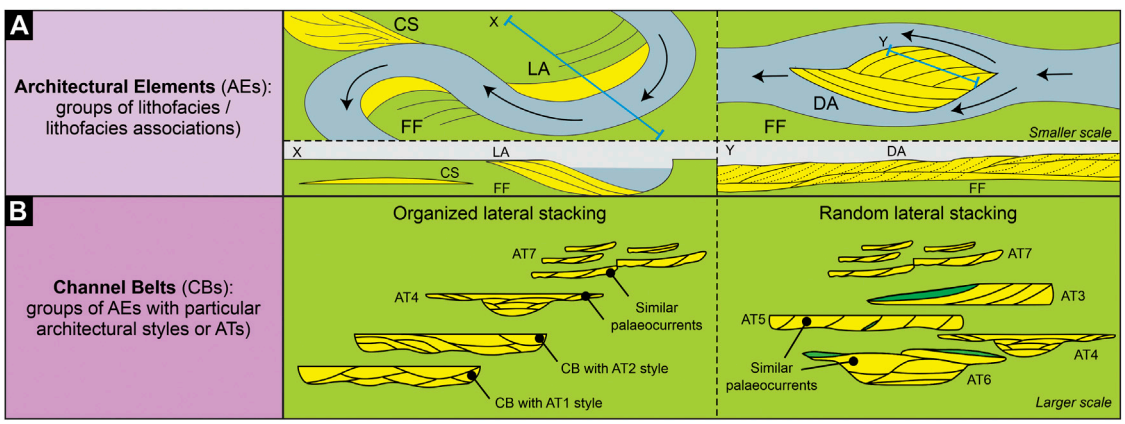

FIGURE 2 | Spatial arrangement of some basic building blocks in the fluvial architecture in this study. **(A)** Architectural elements (AEs), which are groups of lithofacies or lithofacies associations (partially adapted from Gulliford et al., 2014). **(B)** Channel belts (CBs), which are groups of AEs with particular architectural style (abbreviated as ATs in this study). For the details on the ATs, see text, **Table 3**, and **Figures 6**–**8**. Note that these are only schematic, hypothetical representations of the architecture, meant to signify the hierarchical nature of the building blocks. Identifying the spatial relationships of AEs in the floodplain units (in green in B) is difficult due to the lack of high-quality exposures of the fine-grained sedimentary rocks in the MKB. For other abbreviations, see **Table 1**.

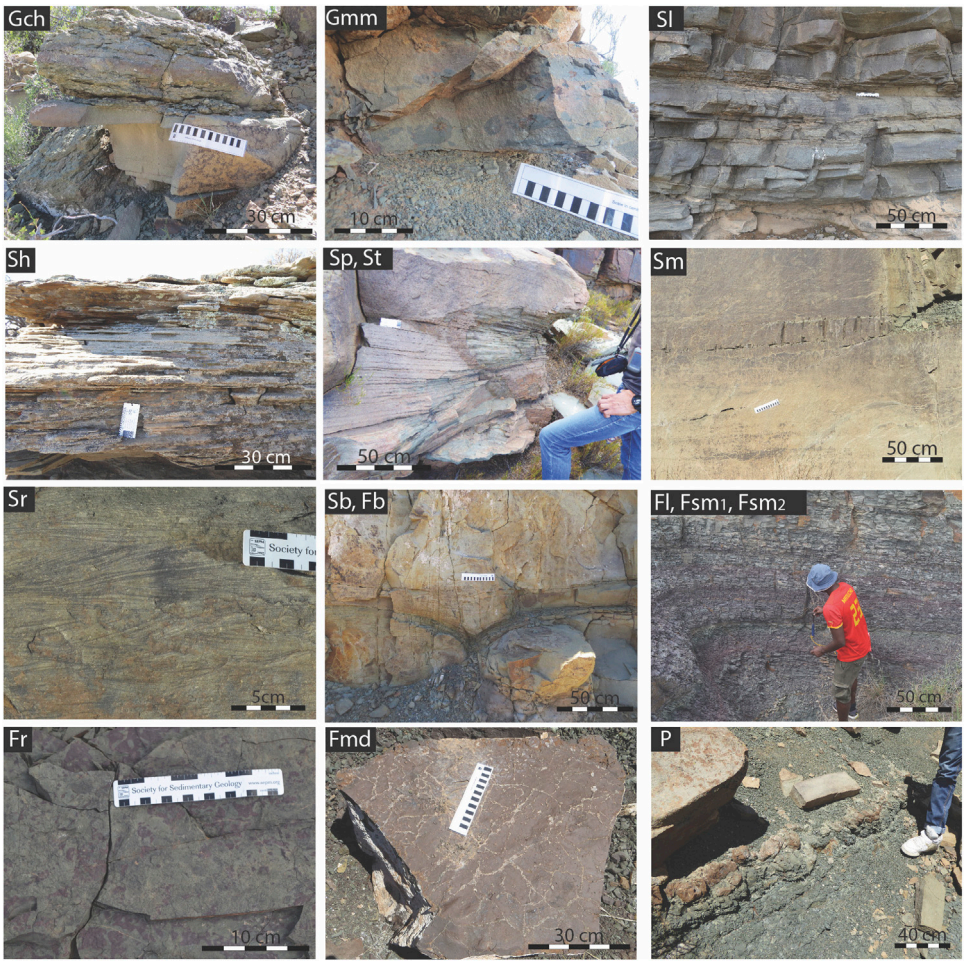

FIGURE 3 | Lithofacies types and their codes: Gch: gravel, clast-supported, horizontally bedded with imbrications; Gmm: gravel, matrix-supported, massive with intraformational, rip-up mudstone chips (code also used for massive, clast-rich sandstone); Sl: low-angle cross-bedded sandstone; Sh: horizontally laminated sandstone; Sp/St: planar/trough cross-bedded sandstone; Sm: massive sandstone; Sr: ripple cross-laminated sandstone with flaser bedding; Sb: soft sediment deformation in sandstone; Fb: soft sediment deformation at the mudstone-sandstone interface; Fl: laminated red-maroon and green-grey siltstone; Fsm1: massive red-maroon mudstone; Fsm2: massive green-grey siltstone; Fr: bioturbated (rootlets only) and/or color mottled texture of the green-grey silt and purple-red mudstones; Fmd: sand-filled desiccation cracks in mudstone; P: paleosol with *in situ* carbonate nodules.

fines" (FF) in **Figure 2A**. The description and quantification of the AEs in our study area are presented in **the Results**.

Higher up in the fluvial architectural hierarchy, the AEs (and their building blocks, the lithofacies) can be contained within channel belts (CBs) that are a few to 10s of meters scale depositional units (**Figure 2B**). Channel belts can be constructed from one or more storeys of smaller channels and other AEs that can be vertically and/or laterally stacked (i.e., multistorey and multilateral; Gibling, 2006). In our simplified sketch of the hierarchal scheme (**Figure 2**), we do not differentiate between single versus multistorey CBs, but attempt to show how the CBs can have variable internal architectures that result from the different proportions and spatial arrangements of the AEs (i.e., Das and LAs) that formed within the paleo-river channels. The architecture of the channel belts is discussed in more detail in **the Results**. In our system, the genetic counterpart of sandstone-dominated CBs comprises those AEs (i.e., levees, crevasse splays, and floodplain fines) that formed adjacent or away from the paleo-river channels in the overbank areas (for details, see, e.g., Miall, 1996; Colombera et al., 2013; Gulliford et al., 2014; Wilson et al., 2014). For simplicity, our catch-all term for these facies associations that are dominated by fine-grained rocks and which occur outside the CBs is floodplain units (FUs; green in **Figure 2**). In general, it is difficult to decipher architecture of FUs because these, being normally mudstone-dominated, are not exposed well enough to establish the bounding surfaces and 3D geometric relations of the facies groups that build them.

RESULTS

Lithofacies

The lithofacies types in this study are illustrated in **Figure 3**. The distribution of the lithofacies over the study area sectors (W1, W2, and E) and within the two formations is shown in **Table 2**,

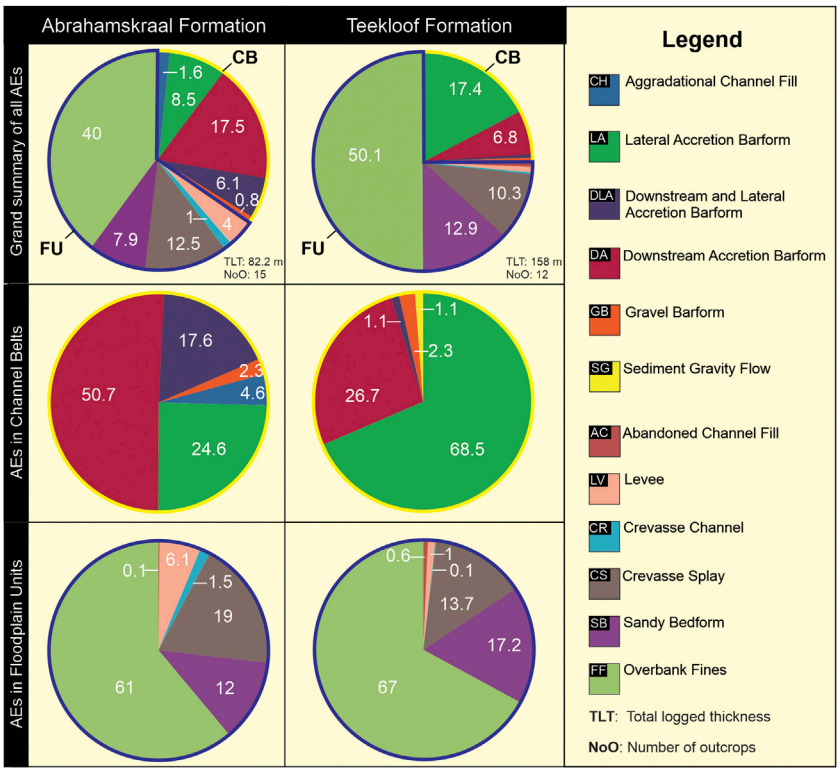

FIGURE 4 | Summary pie charts of the quantitative facies analysis results for the architectural elements in the studied stratigraphic interval. For summary data, see **Supplementary Table S2**. See text, **Tables 1, 3**, and **Figures 6–8** for details. All values are in %-es. Abbreviations: CU: channel belts; FU: floodplain unit; AEs: architectural elements.

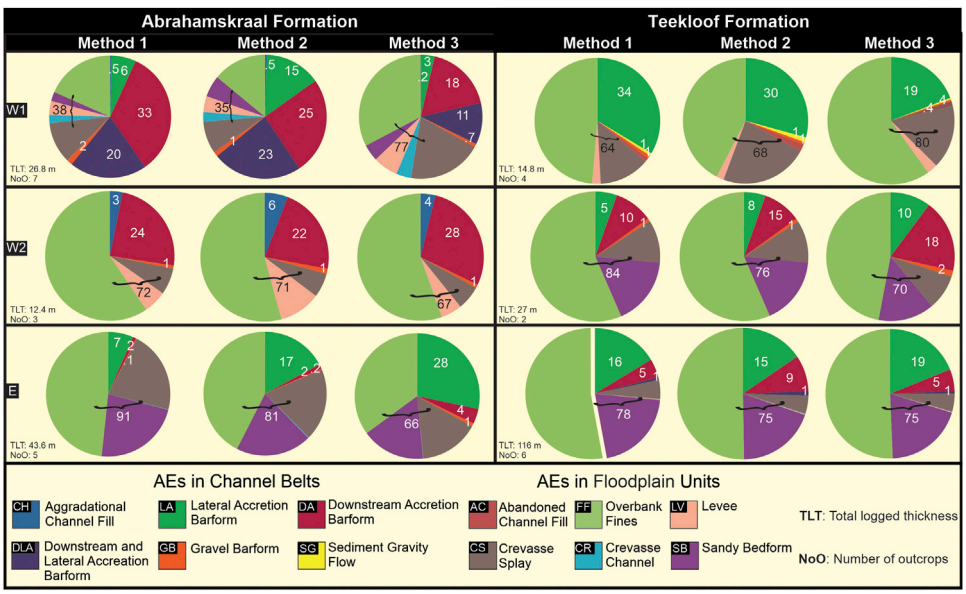

FIGURE 5 | Quantitative facies analysis results for the architectural elements in upper Abrahamskraal and lower Teekloof Formations. Results were compiled from all outcrop facies maps recorded in the study and vary for the three different averaging methods applied (see text and Paiva, 2016). Also, note that percentages for AEs in the floodplain units might have low accuracy due to generally lower quality exposures of the mudstone-dominated units. Abbreviations: AEs: architectural elements; W1: eastern and W2: western sector in the southwestern main Karoo Basin; E: southern main Karoo Basin. See **Figure 1** for the relative positions of W1, W2, and E.

and a more detailed account of the lithofacies types per study area sectors is described in the **Supplementary Material**. The classical interpretation of the fluvial lithofacies is also presented in **Table 2** and is based on generation of fluvial sedimentological studies summarized by, for example, Miall, 1996; Allen, 1970, Allen, 1983; Blatt et al., 1972; Harms et al., 1982; Stear, 1985; Miall, 1985. Herein, we only present a general summary of the sedimentological findings based on the frequency of their occurrences. The upper Abrahamskraal and lower Teekloof Formations are dominated by lithofacies indicative of low energy fluvial processes and comprise alternating successions of laminated purple-red (Fl1) and massive olive green-grey (Fsm2) siltstones. Lithofacies related to tractional processes are characterized by cross-bedded (St, Sl, and Sp), fine-grained, light brown sandstones. Channel deposits in the studied interval of the Lower Beaufort Group are volumetrically dominated by sandstone facies that are organized in classical upward-fining successions, in which the facies are often found in a vertical succession that comprises volumetrically subordinate but common gravel facies (e.g., Gmm1) and/or facies Sl/St at the base, followed by Sp, Sh, Sm, and then Sr at the top. Intraformational clasts within gravel facies are presumed to be locally sourced or have a short travel distance and mostly resulted from ripping-up of nearby floodplain deposits (Stear, 1985). The upward-fining successions, typical if not ubiquitous in fluvial systems, indicate an overall gradual decrease in channel flow energy due to various controls that act on different timescales (Miall, 1985 and Miall, 1996). These include spatial decrease in flow energy associated with the energy dissipation linked with helical flow in sinuous, asymmetrical, and laterally migrating channels (i.e., point-bar migration; Allen 1970), sudden channel plugging during major floods, and/or progressive channel abandonment during avulsion (Allen, 1983; Miall, 1985; Miall, 1996, p. 136, 150). In the S-MKB, medium-grained sandstones are more common throughout the channel deposits, indicating an overall high energy, tractional flow condition for both formations. Gravel facies (**Table 2**) are more common in the upper Abrahamskraal Formation than in the lower Teekloof Formation, suggesting that the upper Abrahamskraal Formation formed under relatively high energy conditions (since the supplied sediment type and direction did not change–see **section on Provenance History**). This overall higher energy fluvial system may be explained by the Abrahamskraal having been deposited, relative to the Teekloof Formation, on a higher gradient regional paleoslope or under climatic conditions with higher energy discharge processes (e.g., higher magnitude flash flood events and plastic debris flows; cf. Miall, 1985).

The interbedding of the green-grey (Fsm2) and the purple-red (Fl1) fines facies is a characteristic feature in the Lower Beaufort Group. Wilson et al. (2014) explain this bed-scale color variation by expanding on the standard conceptual model for coloration of continental red beds (Walker, 1976; Parrish, 1998, but see Sheldon, 2005). According to Wilson et al. (2014), bedding parallel-color banding in the Lower Beaufort Group is linked to seasonal fluctuations in the water table under hot, semi-arid conditions. In their explanation, grey-green coloration indicates reducing (anoxic) subaqueous and high groundwater conditions in contrast to the purple-red coloration that originates in oxidizing subaerial and low groundwater conditions. Furthermore, they consider the thicker red mudstone units a reflection of the "dominance of subaerial arid conditions"; however, coloring of sedimentary rocks has been repeatedly shown to be an unreliable dryness indicator (see, e.g., Sheldon, 2005). Therefore, we consider the common *in situ* carbonate nodules in paleosols and the associated desiccation cracks as more reliable indicators of the paleoclimatic setting, where prolonged and repeated wetting and drying events occurred under hot, semi-arid conditions. In addition, the above sedimentary features (i.e., desiccation cracks, roots, bioturbation, and mottling of colors) collectively indicate weak hydromorphic pedogenic processes and decreased clastic sedimentation rates (Wright and Marriott, 1993; Wright and Marriott, 2007; Slate et al., 1996; Kraus, 1999; Retallack, 2005). The modern counterparts of these soils are characterized by grey/green and red color mottles and may contain nodular or massive hydromorphic carbonate precipitates (Slate et al., 1996). In dryland settings, these soils have also been linked to saline and alkaline shallow groundwater, which has considerably variable redox behavior, and can cause localized (mottling) or stratum-wide color changes in the sediment (Pimentel et al., 1996).

Facies Associations

As explained above, recurring 3D lithofacies associations are the fluvial architectural elements (AEs). The types of AEs in this study correspond to those defined in Colombera et al. (2013) and are described in **Table 1**, which details the geometry, lithofacies content, and origin of the architectural elements. The outcrop lithofacies maps derived from the thirty-five high-quality exposures in this study allowed 1) the confident identification of the AEs; 2) the spatial distribution of the AEs in the outcrops, and 3) the quantification of the relative proportions of the AEs in the studied stratigraphic interval. To derive the percentages of AEs in each exposure of the studied interval, after identifying AEs in each outcrop, we measured, with the aid of ImageJ freeware, the surface area of each AE on the outcrop lithofacies map. To limit sampling bias and errors in the results, we used three different methods of averaging the proportions of the AEs (see Colombera et al., 2013 and Paiva, 2016 for details).

Downstream and lateral accretion architectural elements (DAs and LAs, respectively) are the most abundant AEs in the channel belts in the Lower Beaufort Group (**Figure 4**) and indicate the predominance of rivers with mobile channels. In identifying the DA, DLA, and LA elements (**Table 1**), we measured the angle between paleoflow direction and the orientation of accretionary dip because these angular differences are linked to variations in fluvial style and are key in reconstructing fluvial paleo-environments (Miall, 2010, p. 116). Gradations between DA, DLA, and LA elements are typical (Miall, 2010), and our predefined angles used to distinguish DA from DLA and DLA from LA are 45° and 60°, respectively. The high proportion of DA elements (~50%) in the upper Abrahamskraal Formation can suggest high energy, low sinuosity channels (**Figures 4**, **5**). In the lower Teekloof Formation, the dominance of LA elements (~70%) indicates the lateral migration of point bars, which are common in low

TABLE 3 | Description of the architecture types (ATs) of the channel belts in the studied stratigraphic interval. The individual ATs are illustrated in **Figures 6–8**. For their stratigraphic and regional distribution, see the Discussion and **Figure 9**.

AT	Description of geometry and architectural element content	Illustration
AT1	DA-dominated, sheet/ribbon-like channel belt. Generally has a wavy erosional base with 1–2 m relief and a flat-top with occasional top scour structures. Width: 80 m; thickness: 4 m	**Figure 6A**
AT2	Similar to AT1, but dominated by a mixture of DA and DLA elements. Width: 150 m; thickness: 5.2 m	**Figure 6B**
AT3	Concave-up, ribbon/sheet channel belt; dominated by LA elements, but DA elements are found locally. Floodplain elements fill up the concave-up shape. Width: 70 m; thickness: 4.5 m	**Figure 6C**
AT4	Ribbon-shaped channel belt; dominated by DA elements. The central concave-up scour structure is aggradationally filled by DAs; often with attached wings (i.e., levees) and floodplain elements forming a flat top. Width: 36 m; thickness: 5.2 m	**Figure 7A**
AT5	LA-dominated, sheet-like, flat-topped channel belt. Wavy erosional base with 1–2 m relief; floodplain elements often bound LA elements and also forming the flat top. Width: 100 m; thickness: 3.5 m	**Figure 7B,C**
AT6	Vertically stacked, valley-shaped, ribbon-like channel belt. Dominated by DA elements, but LA elements are found locally, mostly in the upper portion of the belt. Width: 150 m; thickness: 50 m	**Figure 8A**
AT7	Multiple sheets and ribbons, with multilateral and vertical juxtapositions. Dominated by LA elements, but DA elements are found locally. Width: 130 m; thickness: 40 m	**Figure 8B**

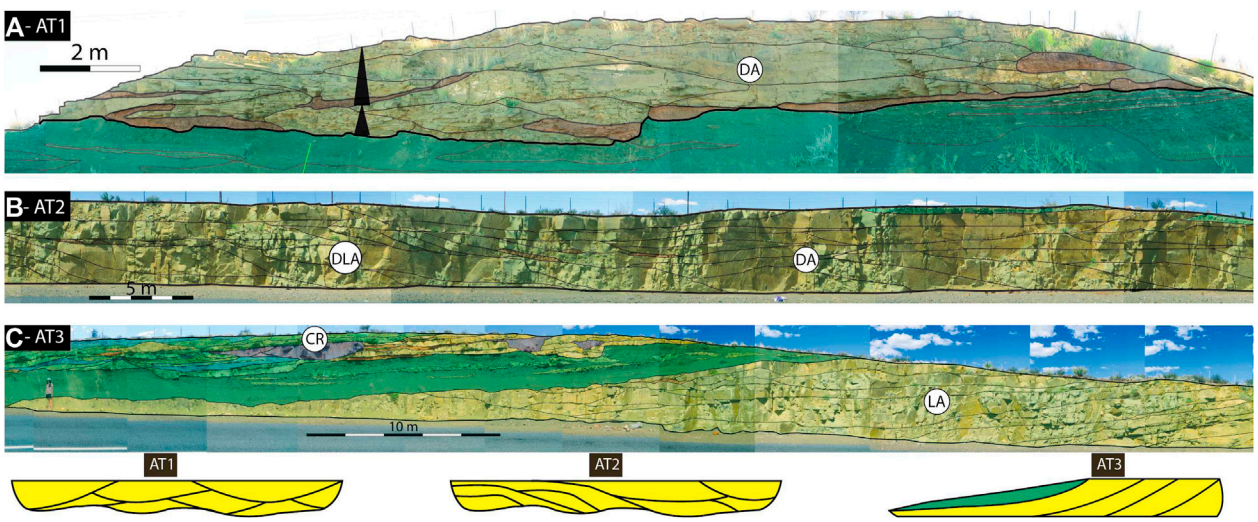

FIGURE 6 | (A) Architecture type 1 (AT1) shown here occurs in a channel belt entirely composed of DA elements. Note the characteristic irregular, erosional base. **(B)** Architecture type 2 (AT2) is similar to AT1 but consists of a combination of DLA and DA elements, and occasionally LA elements. **(C)** Architecture type 3 (AT3) is a channel belt of sheets/ribbons with a characteristic concave-up top surface. AT3 is dominated by LAs, but few DAs are also encountered.

energy, high sinuosity channels. In both formations (**Figures 4**, **5**), crevasse splays (CS) and sandy bedform (SB) elements make up 30% of the floodplain successions (although undeniably distinguishing between these two elements is often difficult–see Miall, 1996, p. 146, North and Davidson, 2012). Furthermore, in the S-MKB, element LA is in essence equally common in both formations, and this may suggest a regional W to E lateral difference in the fluvial dynamics and channel patterns in the upper Abrahamskraal Formation (i.e., mainly higher energy, lower sinuosity channels in the SW-MKB compared to the S-MKB).

Quantification of Architectural Elements

The results from the quantification of the architectural elements (AEs–**Table 1**) in the study area are explained below in stratigraphic order because the ultimate aim of this study is to assess whether or not any systematic facies change occurs across the Abrahamskraal-Teekloof formational boundary, which is considered to represent the end-Capitanian mass extinction event in the main Karoo Basin. The results from the quantification of the AEs are displayed in **Figures 4**, **5** and **Supplementary Table S2**, where we distinguish between AEs associated with coarse-grained, sandstone-dominated facies associations (mostly formed within channels) and fine-grained, mudstone-dominated facies associations (mostly formed on the floodplains; **Figure 2A**; **Table 1**). Thickness and width data of the outcrops used in the quantification of the AEs are in **Supplementary Table S3** (also see **Figures 4**, **5**). For the Abrahamskraal Formation, the data are based on 15 outcrops with a total logged thickness of 82.8 m, whereas for the

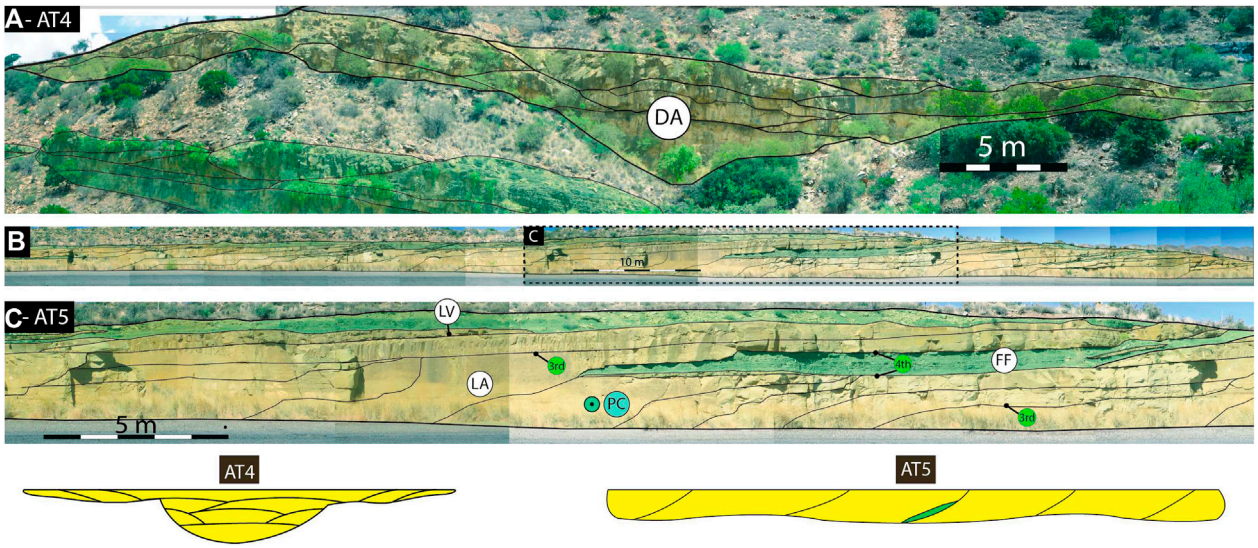

FIGURE 7 | (A) Architecture type 4 (AT4): channel-shaped ribbons, dominated by DA elements. **(B), (C)** Architectural type 5 (AT5): sheet-like channel belt entirely composed of lateral accretion (LA) elements, separated by thin, laminated mudstone layers. Note that the paleocurrent direction (PC) is perpendicular to the outcrop in **C**.

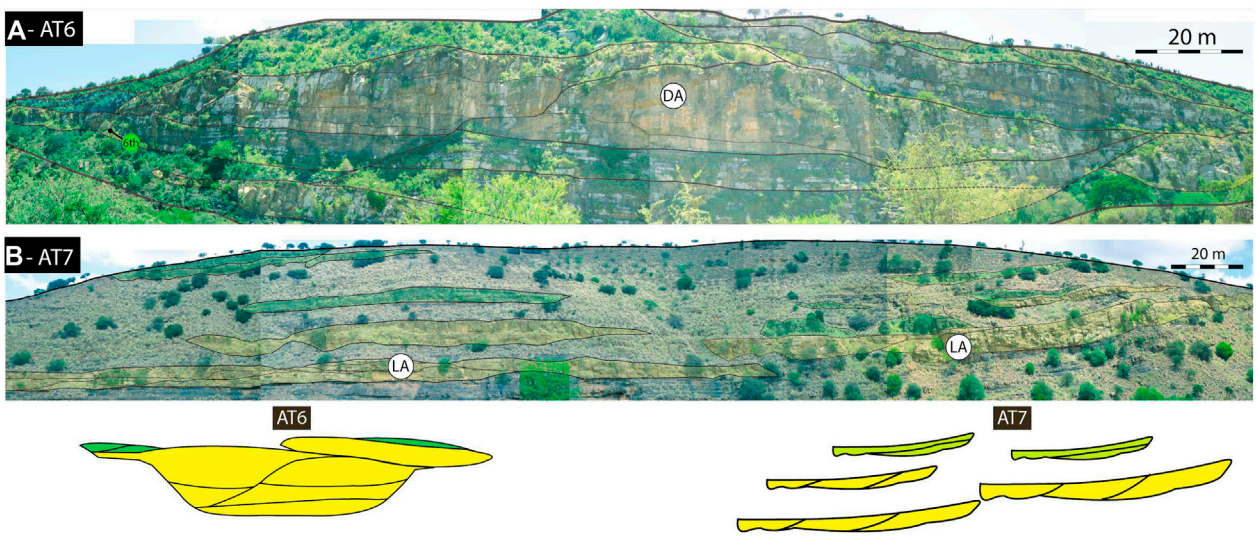

FIGURE 8 | (A) Architecture type 6 (AT6): ribbon-like, vertically amalgamated channel belt. This very thick (~50 m) AT6-dominated unit indicates high aggradation and/or reoccupation rates. **(B)** Architecture type 7 (AT7): channel belt with multiple LA-dominated, sheets and ribbons displaying multilateral and vertical juxtaposition.

Teekloof Formation, the data were obtained from 12 outcrops with a total logged thickness of 158 m. Note that the highest total logged thicknesses for both formations are from the eastern study area (marked as "E" in **Figures 1**, **5**), where thicknesses of 43.6 m (in five outcrops) and 116.2 m (in six outcrops) were logged in the Abrahamskraal and Teekloof Formations, respectively.

Upper Abrahamskraal Formation

Accounting for ~40% of the studied interval, FF (aggradational overbank fines) is the most common AEs across the study areas (**Figure 4**, **Supplementary Table S2**). Other common floodplain-related AEs are levees (LV: 4%), crevasse splays (CS: 12.5%), and sandy bedform (SB: 7.9%). Channel-related AEs, making up ~35% of the formation, are dominated by downstream accretion elements (DA: ~17.5%), downstream and lateral accretion elements (DLA: ~6.1%), and lateral accretion elements (LA: ~8.5%). Although rare (0.8%), the presence of the Gravel Bar (GB) element is ubiquitous at the base of the channels across the study areas. It is noteworthy that the abundance of element DA (average ~25%) in the SW-MKB (W1, W2 in **Figure 1**) sharply declines to only 2% in the

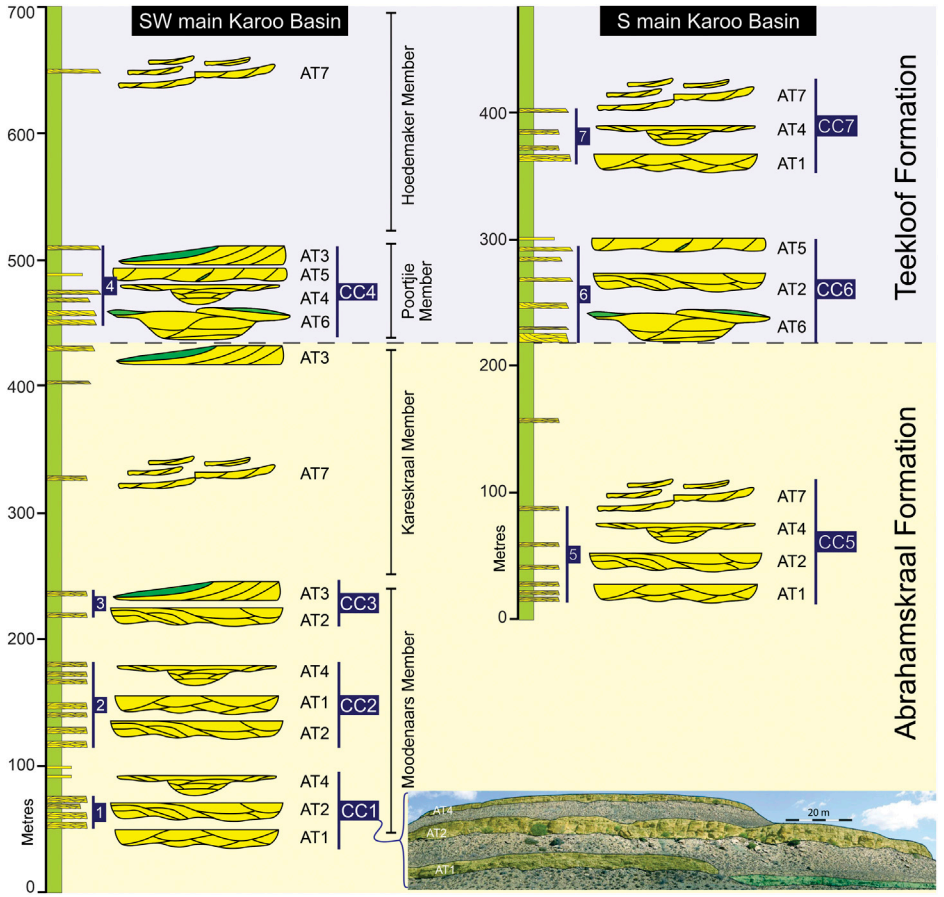

FIGURE 9 | Stratigraphic context of the channel-belt clusters (CCs) and the main architecture types (AT) of the channel belts (CBs) that build the CCS, in the SW-MKB and S-MKB. For the detailed description and illustration of the ATs, see **Table 3** and **Figures 6**–**8**. The lower right inset shows part of channel-belt cluster 1 (CC1), which is defined by a group of four channel belts (CBs–see log), which are vertically closely spaced, genetically related, but architecturally different from each other as the lowermost CB has AT1, the middle CB has AT2, and the upper two CBs have AT4. Note that the uppermost, fourth CB in CC1 is not shown in the photo. Scale provided is approximate. Correlation of the CCs is not possible across the study region that is ~600 km long (see **Figure 1**).

S-MKB (E in **Figure 1**), where the channel belts are dominated by LAs (17.4%; see **Figures 4**, **5**). Furthermore, the abundance of DLAs decreases from ~18% in area W2 to 0% both towards the east (E) and west (W2). In other words, unlike in the SW-MKB, the upper Abrahamskraal Formation is dominated by element LA (and not element DA or DLA) in the S-MKB; however, it is worth noting that in the S-KKB fewer outcrops were available for quantification than in the SW-MKB.

Lower Teekloof Formation

Aggradational overbank fines (FF) element constitutes up to 50% of the Teekloof Formation in the studied interval (**Figure 4**, **Supplementary Table S2**). Other common floodplain-related AEs are crevasses splays (CS: 10.3%) and sandy sheet-floods (SF: 12.9%). The Teekloof Formation is dominated by LAs (~17.4%), contains some DAs (0% in W1, 14.2% in W2, and 6.3% and E), and lacks element GB in E, which is otherwise present, but very rare in the SW-MKB (**Figures 4**, **5**). Generally, elements DA and DLA are very rare in the lowermost Teekloof Formation, and element LA is in essence equally common in both formations (**Figure 4**).

To sum up, the main difference between the two formations is in the ratio of DA to LA being 2:1 and 1:2.5 in the Abrahamskraal and Teekloof Formations, respectively, which implies an upward increase in channel sinuosity. The proportions of the channel and floodplain deposits vary for both formations within the western study area (W1 and W2) as well as from SW-MKB to S-MKB (**Figures 4**, **5**). This ratio is 1:1 and 2:3 in W1 and W2 areas, respectively, for the Abrahamskraal Formation and is 2:3 and 1:3 in W1 and W2 areas, respectively, for the Teekloof Formation. Overall, the ratio is 2:3 and 1:3 for the Abrahamskraal and Teekloof Formations (**Figure 4**), respectively. While the ratio stays constant in the Teekloof Formation across the MKB, in the Abrahamskraal Formation, this ratio is 2:3 in SW-MKB and 1:4 in S-MKB. This reflects the overall dominance of floodplain-related AEs in both formations as well as a general increase in their abundance across the contact of the Abrahamskraal and Teekloof Formations (i.e., upward decrease in sandstone fraction).

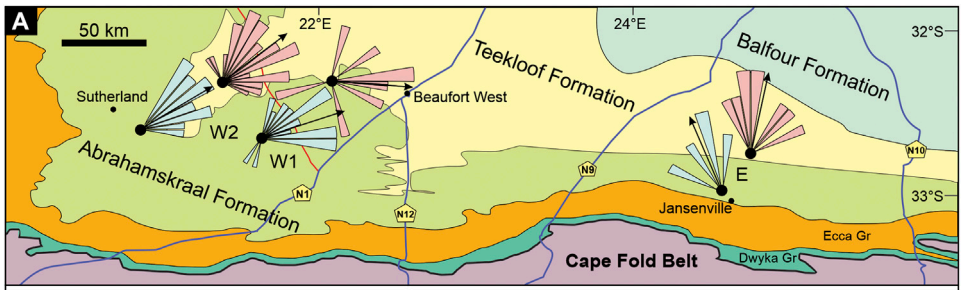

	Abrahamskraal Formation			Teekloof Formation		
	W1	*W2*	*E*	*W1*	*W2*	*E*
Number of Readings	31	18	5	8	54	9
Mean Direction (°)	71.3	58.7	336.1	93.8	51.9	12.2
Vector Magnitude	25.1	17.1	4.56	4.34	46.9	8.06
Consistency Ratio	0.81	0.95	0.91	0.54	0.87	0.90
Standard Deviation	35.4	18.0	24.0	54.8	29.2	26.2

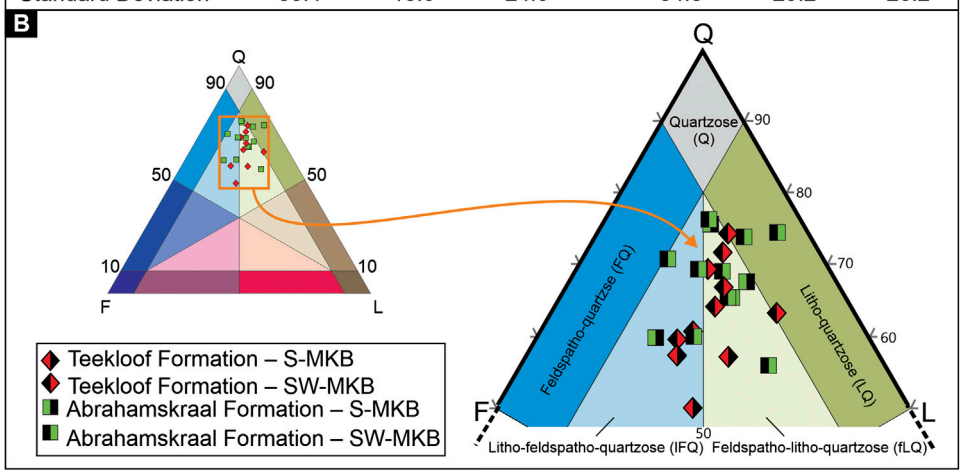

FIGURE 10 | Provenance diagrams. **(A)** Paleocurrent rose diagrams of the upper Abrahamskraal (blue) and lower Teekloof (pink) Formations show that the source areas were persistent through time and in both the SW-MKB and S-MKB. Abbreviations: W1: eastern and W2: western sector in the SW-MKB; E: S-MKB. The paleocurrent data were obtained from various beds in the different CCSs, but because individual CCSs provided statistically insignificant number of measurements, the roses show the summary data for the formations. The variability within the dataset is reflected by the consistency ratio, also known as the vector dispersion (= R/n, where R is the length of the resultant vector and n is the number of measurements). **(B)** Quartz-Feldspar-Lithic (QFL) ternary diagram shows the composition of the upper Abrahamskraal (squares) and lower Teekloof (circles) Formations samples, which are quartz-rich sandstones. Note that the composition and sandstones (thus likely their source) remained unchanged throughout the depositional history of the studied interval. Classification scheme after Garzanti (2019). Note that the main diagram only shows sandstone fields with >50% quartz content and is adapted from inset ternary diagram, where the clustering is more evident (orange circle).

Channel Belts and Their Clusters

Within each channel belt (CB) in the studied stratigraphic interval, the architectural elements appear to occur in recurrent combinations. The recognition of these recurring motifs of the AEs within the CBs leads to the definition of seven different architectural types (ATs) in the channel belts of the study area with each AT having a distinct external morphology and internal make-up of architectural elements (**Table 3**; **Figures 6–8**). In other words, similar to the concept of AEs containing building blocks of recurring lithofacies associations, the ATs, which are one order of magnitude larger (10–100 m scale), are composed of one or more recurring AEs (**Figure 2B**). Our architectural type concept resembles the "Architectural Styles" of Wilson et al. (2014); however, that approach defines the styles across fluvial hierarchical categories and is not embedded into a robust stratigraphic framework (i.e., in their study, the position of the "Architectural Styles" within the local stratigraphy is poorly defined). To determine the position of a given channel belt within the overall stratigraphic framework of the Lower Beaufort, we used litho- and biostratigraphic boundaries as guides (regional datum). These boundaries are well-established stratigraphic contacts that were mapped by several generations of geologists and paleontologists.

The architectural types of the channel belts in the upper Abrahamskraal Formation are AT1, AT2, and AT4 (AT5 and AT6 are absent), whereas the lower Teekloof Formation channel belts show mainly architectural types described as AT4, AT5, AT6, and AT7 (**Table 3**; **Figures 6–8**). Architecture type AT6 (**Figure 8A**; **Table 3**), an up to 50 m thick, amalgamated sandstone channel belt in the lower Teekloof Formation in

both study areas, represents a departure from the dominant architecture type (A5 and less so A4) and typical thickness of the channel belts in the formation. This architecture type has also been reported before in the Lower Beaufort Group (Gulliford et al., 2014; Wilson et al., 2014) and can be explained by products of relatively high energy fluvial systems with frequent channel reoccupation rates and strong scouring power (i.e., due to base level drop according to Wilson et al., 2014).

Some of the CBs in the studied stratigraphic interval appear to form groups of channel bodies that are separated vertically by up to ~10 m fine-grained deposits. These clusters of CBs are termed here "channel-belt clusters" (or CCs; **Figures 2**, **9** and inset detailing CC1). The component CBs grouped together in any given CC differ from each other architecturally, as each CB is made up of recurring groups of architectural elements, defined in this study as architectural types (ATs; for details, see **Table 3**, **Figures 2**, **6**–**9**). In any given CC, the number of CBs ranges from two to seven (e.g., CC1 comprises 4 CBs–see inset in **Figure 9**). While some CBs may form random lateral stacking in the studied stratigraphic interval, most CBs are laterally offset within a given CC (left panel in **Figure 2B**), and this way, each of the CCs is laterally traceable for several kilometers in the field.

Because no outcrop shows all CCs at once, the relative stratigraphic order of the seven CCs (as shown in **Figure 9**) identified in this study was established by careful field mapping that involved the critical assessment of the relative distance of each CC from the key formational boundaries, and this was aided by both lithostratigraphic and biostratigraphic proxies. This way the CCs are embedded into the local stratigraphic framework in each of the study areas, and thus their comparison across the study region can be made with confidence (see below). It is worth nothing that correlation of the CCs across the study region was not attempted because no CC is traceable for several hundreds of kms. However, the regional comparison of the CCs, as detailed below, is necessary for 1) a more accurate interpretation of the depositional processes through this critical Permian interval and 2) summarizing the general depositional trends in the SW-MKB and S-MKB.

Of the four channel-belt clusters in the upper Abrahamskraal Formation (**Figure 9**), three (CC1, CC2, and CC3) are in the SW-MKB, and one (CC5) is in the S-MKB. Of these, CC1, CC2, and CC5 comprise architecture types AT1, AT2, and AT4, whereas CC3 contains architecture types AT2 and AT3 (**Table 3**; **Figures 6**, **7**). Architecture types AT5 and AT6 are not found in the studied stratigraphic interval, and AT3 is very rare and only found in the SW-MKB close to the upper contact of the formation (**Figure 9**). Of the three channel-belt clusters in the lower Teekloof Formation (**Figure 9**), CC4 is in the SW-MKB, and CC6 and CC7 are in the S-MKB. The common architecture types are AT4, AT5, AT6, and AT7 (**Table 3**; **Figures 7**, **8**), of which AT5 and AT6 seem to be diagnostic to the lowermost Teekloof Formation in both SW-MKB and S-MKB. The architecture types rarely encountered in the lower Teekloof Formation are AT1, AT2, and AT3 (**Figure 9**). Notwithstanding the fewer outcrops in the S-MKB, it is important to note that here the two formations are set apart by architecture types, that is, AT5 and AT6, which are considered diagnostic of the lowermost Teekloof Formation (**Figure 9**).

Provenance History

The results of the paleocurrent analysis are summarized in **Figure 10A**. Mean paleocurrent directions in the SW-MKB indicate paleocurrents from roughly the southwest to the northeast for both formations. The exception being at location W1 of the Teekloof Formation, where the flow direction is roughly from W to E. Significant differences are found in the vector magnitudes (25.1; 4.3) and consistency ratios (0.81; 0.54) at W1 location for the upper Abrahamskraal and lower Teekloof formations, respectively. At W2 location, the more robust datasets for both formations provide more confidence in the results. The main flow direction for both units is from SW to NE; the consistency ratios and vector magnitudes are relatively high. This result agrees with previous paleocurrent studies in the region (Cole and Wipplinger, 2001; Gulliford et al., 2014; Wilson et al., 2014). In the S-MKB, the paleocurrents were from the south to the north; however, the confidence in this result is low because only a limited number of measurements (n = 14) could be obtained in this area.

The petrographic composition of the sandstones (**Figure 10B**; see **Supplementary Table S4** for raw petrographic data), derived from the thin section analysis via Gazzi-Dickinson point-counting method, shows no spatiotemporal changes but rather a distinct clustering in the quartz-rich fields (Q: ~50–<80%; F: 5–30%; L: 10–35%). In the descriptive petrographic classification of Garzanti (2016) and Garzanti (2019), according to which the samples are mainly litho-feldspatho-quartzose (lFQ) and feldspatho-litho-quartzose (fLQ) sandstones (**Figure 10B**), only three samples are litho-quartzose (LQ) sandstones; these were taken in the SW-MKB. The petrographic study relevant for provenance also showed that 1) our fine-grained sandstone samples contain, mainly, subrounded grains and are generally submature with an >15% of clayey matrix (occasionally up to 30%), 2) the Teekloof Formation samples appear to be very slightly richer in feldspars (av. ~18%, range ~9–25% vs. the very slightly more mature Abrahamskraal Formation with an av. feldspar content of ~13%), and 3) feldspar grains tend to be fresh (i.e., not altered) in most samples.

Paleocurrent results (**Figure 10A**) show two distinct sediment transport directions from the SW and S in the SW-MKB and S-MKB, respectively, for both formations. With the Abrahamskraal Formation being only slightly more quartz rich compared to the Teekloof Formation (av. quartz content 68% vs. 60%, respectively; **Supplementary Table S2**), the petrographical results (**Figure 10B**) are considered very similar for both formations throughout the region and imply a similar sediment source for both the SW-MKB and S-MKB. The results also suggest that the two geographically different sources in the SW and S were petrologically similar if not identical throughout the deposition of the upper Abrahamskraal and lower Teekloof Formations. Collectively, these suggest that the sediment source was the laterally extensive orogenic area of the CFB to the SW and S of the study region (**Figure 1**). The data did not allow to further refine the geological make-up of source terrains in the SW and S. Similarly, the limited nature of the dataset cautions us against speculating about the small differences in the petrographic data

that could have resulted from potential differences in paleohydraulics as well as weathering at source area, during transport, sedimentation, post-burial diagenetic modifications, etc. (Weltje and von Eynatten, 2004; Garzanti, 2016). However, because within the study area sectors (W1, W2, and E) the paleocurrents are constant across the studied stratigraphic interval, it is reasonable to assume that the direction of the main paleoslopes in the Cape Orogen remained essentially the same during the end-Capitanian. Furthermore, in both facies areas, the change in rock composition appears to be insignificant across the contact of the upper Abrahamskraal and lower Teekloof Formations. These trends indicate stability not only in the sediment transport direction through time, but also in petrological composition of the source area (i.e., Cape Orogen) and potentially in the prevailing climate (see Paiva, 2016 for major and trace element geochemical results supporting this latter inference). Therefore, it can be concluded that the observed spatiotemporal architectural differences across the formations are probably not linked to changes in the composition and position of the provenance area and/or climate, but are more likely reflective of specific geomorphic changes due to autogenic and/or tectonic (allogenic) controls (see Discussion).

DISCUSSION

Change in the Fluvial Architecture

Our observations show subtle changes in the fluvial architecture across the boundary of the older upper Abrahamskraal and younger lower Teekloof Formations and include (from bottom to top) 1) a change in architectural type of the channel belts from DA- to LA-dominated; 2) a slight decrease in the abundance of gravelly facies especially in the SW-MKB; and 3) a slight increase in the abundance of floodplain architectural elements in both regions (**Table 2**, **Figures 4–9**). We explain these vertical trends, which overall amount to a retrogradational stratigraphic pattern, to reflect an overall up-section increase in channel sinuosity and concomitant overall decrease in the environmental energy of the channel processes, as well as changes in aggradation and/or channel reoccupation rates. Specifically, in the SW-MKB, the upper Abrahamskraal Formation contains facies associations indicative of higher energy levels than the lower Teekloof Formation (**Figures 4–9**). Seeing that the paleocurrents patterns and sediment provenance remain the same across the formation boundary, the subtle changes in architecture could be attributed to the lowering in the gradient of the regional paleoslope with time. As represented by the upper Abrahamskraal Formation, the initially steeper paleoslope was dominated in its proximal portion by rivers with higher environmental energy channels. Afterwards, during the deposition of the lower Teekloof Formation, the regional paleoslope became gentler and mostly supported the development of river channels with lower environmental energy but higher sinuosity. Lastly, we suggest that, through the same time interval, the amount of the paleoslope inclination was more pronounced in the SW-MKB than in the S-MKB. In the latter area, the change in the relative proportion of architectural elements in the channel belts is subtle, but the change in architecture types is still evident (**Figures 6–9**). The discrepancy in the abundance of the architectural elements and types between the SW-MKB and S-MKB may be due to the differential subsidence rates across the depositional dip of the basin.

However, the above explanation of the observed fluvial architecture changes by overall lowering of the regional paleoslope gradient (see example above) evokes further

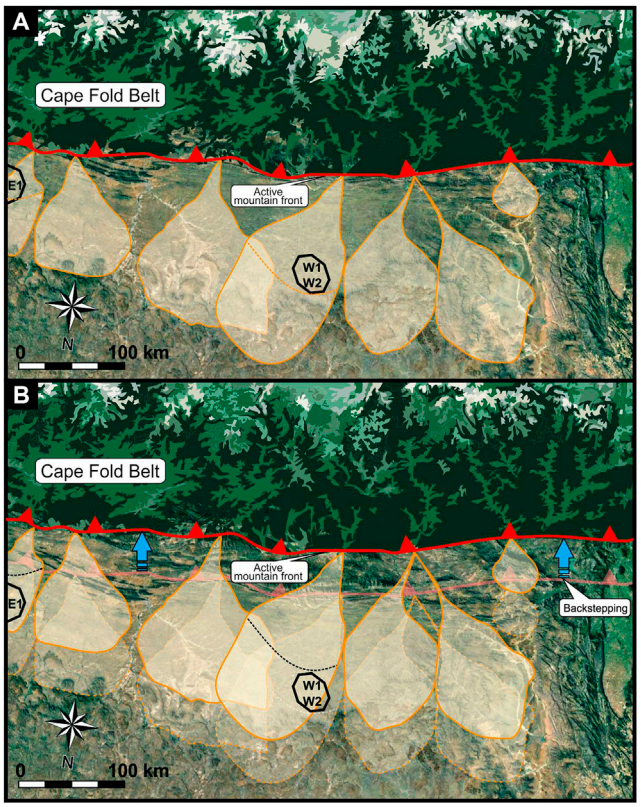

FIGURE 11 | Schematic reconstruction of the regional depositional environment during the accumulation of the upper Abrahamskraal and lower Teekloof Formations in the southwestern and southern main Karoo Basin at the end-Capitanian. Sediment was supplied from the same orogenic hinterland (Cape Fold Belt) throughout the depositional history of the studied stratigraphic interval, which represents the different parts of a multiple megafan system similar in size to the modern megafans south of the Himalayas (see Shukla et al., 2001, figure 1). Abbreviations W1, W2, and E mark the study areas in the southwestern and southern main Karoo Basin, respectively. E is closer to the apex of the megafan in the S-MKB because sandstone bodies there are narrower and thicker. The position of the studied interval (see polygons) on the megafans is shown during deposition of the upper Abrahamskraal **(A)** and lower Teekloof Formations **(B)**. Note the backstepping (blue arrow) of the active mountain front (red line) and retrograding of the megafan system towards south. Black dashed line is the transition between the medial and distal megafan regions (see text for details). The illustration is a compilation from scaled 2016 GoogleEarth© images of the southwestern region of South Africa and the Bihar and West Bengal regions of India, from where the following modern megafan outlines were adopted (from E to W): Gandok, Kosi, Sarda, and Tista (two lobes).

questions: Why did regional slope become gentler with time? How do the different trends in architecture type fit in the larger evolutionary history of the main Karoo Basin? What were the processes controlling the architecture trends? Why do the changes in architecture trends coincide with the mass extinction event reported by Day et al. (2015)? Who also investigated the same stratigraphic interval? While the data presented in this work may not be robust enough to fully address all of these questions, some considerations and conclusions can be drawn from the information available. The retrograding stratigraphic trend will be discussed in the light of autogenic (e.g., avulsion, channel adjustment) and allogenic controls (i.e., eustasy, climate, and tectonics) (**Figure 11**).

Autogenic Mechanisms

Given the size of the study region, the vertical and lateral architectural trends preserved in it, our favored large-scale alluvial model for the Lower Beaufort Group is a megafan system (**Figure 11**). Megafans are fan-shaped alluvial systems that are common in foreland basins, flank orogenic hinterlands, and show, from fan apex to toe, predictable fluvial style zonation (e.g., higher energy, lower sinuosity channels in proximal, straighter channels in medial, lower energy, and higher sinuosity channels in distal zones) and associated facies changes (Singh et al., 1993; Shukla et al., 2001). Megafans are part of a range of distributive fluvial system (DFS) sizes according to Hartley et al. (2010) (p. 171), who refer to megafans as "large DFSs that are greater than 30 km in length." The key characteristics of the large DFS model, that is, an upward increasing trends in grain size, channel deposit thickness, and clustering, have been reported in the Lower Beaufort Group (Gulliford et al., 2014; Wilson et al., 2014). In this way, our interpretation of the succession being part of the megafan system is in line with previous interpretations; however, the above-described subtle vertical change in the fluvial architecture (e.g., **Figures 4**, **5**, **9**, **10**; **Table 2**) befits a retrograding DFS rather than a prograding DFS (Weissmann et al., 2013; Gulliford et al., 2014; Wilson et al., 2014; Owen et al., 2017b; Wang and Plink-Bjorklund, 2019). We further suggest the observed stratigraphic trends in the studied conformable succession mirror deposition on initially more proximal slopes with higher energy and lower sinuosity channels and then on more distal slopes with lower energy and higher sinuosity channels across a dynamic Permian megafan system in the MKB that was retrograding with time. More specifically, we explain the vertical increase in the abundance of floodplain-related AEs as well as LA elements, especially in the SW-MKB, with a decrease in the environmental energy but increase in the sinuosity of the channels due to a possible source-ward retreat (backstepping or retrograding–cf. Miall, 1978; Moscariello, 2018) of the megafan zones at the end-Capitanian. In this depositional model, the DA element-dominated upper Abrahamskraal Formation and the LA-dominated lower Teekloof Formation were part of the medial and distal megafan zones, respectively. If the strata studied, which are conformable (**Figure 1B**), were deposited in directly adjacent areas along the depositional dip (i.e., in the transition from the distal part of the medial to the proximal part of distal zone–**Figure 11**), the retrogradation of the megafans may have been minor given the subtle stratigraphic changes. Backstepping of proximal-to-distal facies zones was also reported by Sinha et al. (2014) in the modern Kosi and Gandak megafans in the Himalayan foreland basin, which are comparable in size to the Permian megafans in the MKB (**Figure 11**—Tandor et al., 2008; Srivastava et al., 2010). The spatial variability in the Himalayan megafan stratigraphy was linked to unspecified "changes in hydrological regime," the geomorphology of the active mountain front, and sediment flux. Our main argument for the backstepping being linked to basin-wide allogenic controls rather than local autogenic processes is that these vertical trends occur in coeval stratigraphic intervals, representing ~2–2.5 myr across the end-Capitanian, in both the SW and S-MKB, which are study areas ~600 km apart.

Allogenic Mechanisms

Eustasy

Base-level changes that are linked to eustasy normally influence fluvial processes within tens of kilometers upstream from the shoreline (i.e., width of buffer zone generally: < 200 km–Blum and Törnqvist, 2000; Holbrook et al., 2006; Blum et al., 2013; Catuneanu, 2019). The fully continental Lower Beaufort Group is conformable with the underlying marine Waterford Formation in the uppermost Ecca Group (Rubidge, 2005); therefore, eustasy-controlled architecture (e.g., incised valleys) would be expected to be present in the lowermost Abrahamskraal Formation. However, it has been well documented that, by the late Capitanian, paleoshoreline within the main Karoo Basin was well over 200 km from the current study areas and was moving towards the NE (Rubidge et al., 2000; Rubidge, 2005). For this reason, the influence of eustasy on the studied interval is not considered important.

Climate

To date, the entire Lower Beaufort Group is thought to have been deposited in a hot, semi-arid climate with limited chemical weathering and low sedimentation rates (Keyser, 1966; Smith, 1979; Smith, 1987; Smith, 1990; Smith, 1993; Stear, 1985; Cole and Wipplinger, 2001). Catuneanu and Elango (2001) and Catuneanu and Bowker (2001) also argued for the lack of climatic changes on the Permian of the MKB and explained the stratigraphic trends as the exclusive consequence of changes in the foreland basin (flexural) tectonics in a setting that was free of marine influences. This view of long-term climatic stability contrasts with the work of Rey et al. (2016), who, based on oxygen and carbon isotopes values from teeth and bone of Karoo continental tetrapod fossils, showed an increase in average temperatures across the Permian and at Permo-Triassic boundary. The details of the Permian climatic events (rate of change, magnitude) and impact on terrestrial ecosystems in the MKB are still under investigation (Day pers. comm.); however, these climate variations, reconstructed from the stable isotope geochemistry of tetrapods, would be expected to have caused lake level fluctuations, which in turn can affect fluvial style as local base level is critical for the fluvial architecture of inland areas

(Catuneanu, 2006). While it is possible that the fluvial architectural change across the Abrahamskraal-Teekloof formational boundary was climatically influenced, the sedimentological and petrographic results reveal a persistent hot, dry climatic signal for the entire studied interval. The climatic signals in the sedimentary facies (e.g., vertical and lateral reoccurrence of *in situ* and reworked carbonate nodules and associated, poorly developed paleosols) observed in this study as well as in earlier research (e.g., Keyser, 1966; Smith, 1979; 1993) support this stable hot, semi-arid climatic setting. Moreover, the major and trace element geochemical study of the exact same interval by Paiva (2016) also confirmed the above semi-arid climatic signal and its persistence up-section. Despite the overwhelming record for this stable semi-arid climate, the evidence for climate change in this paleontologically significant stratigraphic interval needs to be considered in the context of the highly fragmentary fluvial stratigraphic record (Miall, 2014, 2015). Because of this stratigraphic incompleteness, it is possible that evidence for a high magnitude, but short-lived global forcing event(s), will be either unrecorded in an apparently conformable continental succession or undetected by paleoclimate proxy methods that rely on the naturally low-resolution fluvial record. All in all, to demonstrate that the sudden, high magnitude perturbation, or megaevent (Allen, 2008), was captured not only by the fossils, but also by the physicochemical properties of the MKB sedimentary fill, very fine resolution quantitative stratigraphic methods are required that would have higher detection level than those applied in this study.

Tectonics

It is proposed that the stratigraphic trends observed could be primarily driven by tectonics and explained by using the approach of alluvial stratigraphy (Wright and Marriott, 1993; Mackey and Bridge, 1995; Catuneanu, 2006; Zecchin and Catuneanu, 2013; Catuneanu, 2019). This school of thought analyzes stratigraphic trends in terms of rates of accommodation creation (i.e., subsidence) and rates of sedimentation (cf. Bryant et al., 1995; Colombera et al., 2015). In this context, it is possible that subsidence rates increased, albeit at different rate in the SW-MKB vs. S-MKB, during the deposition of the studied interval, which could explain the retrogradation of the facies zones and changes in fluvial architecture (e.g., change from DA-to LA-dominated channel belts especially in the SW-MKB: **Figures 4**, **5**; dominance of AT5 and AT6 in lower Teekloof Formation: **Figure 9**). Considering that no changes in the paleoslope direction and source rock types are detected in the studied interval, the observed fluvial architecture change may have been caused by a minor lowering of the regional paleoslope linking the study area to the active mountain front of the CFB. The current data is insufficient to further describe the tectonic forces in the CFB during the deposition of the studied succession, and thus our results do not lend explicit support for either of the two main contesting basin evolution models of the MKB in the Permian (i.e., subsidence determined by orogenic loading/unloading stages of Catuneanu et al., 1998 vs. extensional adjustments of basement blocks in Tankard et al., 2012). However, forthcoming radiometric dates and further enhancement of the vertebrate biostratigraphic resolution of the studied interval (Rubidge and Day pers. comm.) will allow the better quantification of sedimentation rates, including channel aggradation and amalgamation rates, and further assessment of how the stratal stacking patterns relate to the tectonic control (see the Sedimentation Rate Scale concept in Miall, 2015). Furthermore, more robust calculation of the sedimentation/subsidence rates would also enable the quantification of the link between differential subsidence and fluvial sedimentation style in the Permian (Kraus, 1999; Flood and Hampson, 2015; Dingle et al., 2016), as well as a more meaningful comparison with other more fully quantified alluvial systems (Hirst, 1991; Weissmann et al., 2015; Owen et al., 2015, 2019; Wang and Plink-Bjorklund, 2019).

CONCLUSION

Deposition of the studied ~600 m thick sedimentary succession occurred on tectonically controlled megafans in the MKB at the end of the Capitanian, some 260 Ma ago and over ~2–2.5 myr (**Figures 9**, **11**). Across the boundary of the upper Abrahamskraal and lower Teekloof Formations, our results demonstrate the following main stratigraphic findings:

1. In the channel deposits, an upward decrease in DA architectural elements from ~51 to ~27% and an increase in LA architectural elements from ~9 to 69%, thus suggesting an upward increase in channel sinuosity (**Figures 4**, **5**–although note the regional lateral differences in **Figure 9**).
2. pward increase in the finer grained architectural elements (e.g., FF, CS), which are associated with floodplain deposition (**Figures 4**, **5**, **9**; **Table 3**).
3. Subtle difference in the make-up of the channel-belt clusters, which normally contain flat-topped, low amalgamation, laterally continuous (for 10s of kms), sheet-like channel belts (**Figures 2**, **4**–**9**) in both formations; however, channel belts with architectural styles AT5 and AT6 are only found in the lower Teekloof Formation.
4. Constant directions in paleocurrents (**Figure 10A**), which are NE directed in the SW-MKB and N directed in the S-MKB.
5. Constant sediment provenance as well as similar sandstone composition (**Figure 10B**) and maturity indicative of a persistent orogenic sediment source.

In summary, the results from our multi-proxy sedimentological work reveal persistent sediment sources, paleocurrents, and a subtle change in fluvial architectural style of the channel belts during the deposition of the studied interval in a hot, semi-arid paleoclimate. In particular, the vertical stratigraphic changes in this 600 m thick succession show a stable landscape except for a slight, long-term retrograding stratigraphic trend (i.e., backstepping towards the source). We propose that these stratigraphic trends most likely reflect tectonic action on Permian megafan systems that drained from south to north in the MKB (**Figure 11**). Moreover, while we support the view that the end-Capitanian mass extinction event, which impacted the biodiversity patterns of the same stratigraphic interval (Day et al., 2015), was probably caused by a high magnitude, but short-lived global forcing event (Rey et al., 2016), the changes

caused by this event seem to remain below the detection thresholds of our current multi-proxy methods in the MKB. Therefore, to further quantify how this paleontologically significant Permian (Zhou et al., 2002; Shellnutt et al., 2012; Day et al., 2015; Lucas, 2017) event was recorded in the Karoo rocks, higher resolution stratigraphic studies are required. Alternatively, it is also possible that the global environmental change from this end-Capitanian event (Rey et al., 2016; Huang et al., 2018; Zhang et al., 2019) may have remained uncaptured by the clastic rocks of the MKB, potentially because the fluvial rock record is a "very incomplete recorder of geologic time" and of, geologically speaking, sudden paleoclimatic/environmental megaevents (Allen, 2008; Miall, 2014, Miall, 2015, Miall, 2016, 2017).

DATA AVAILABILITY STATEMENT

All datasets generated for this study are included in the article/**Supplementary Material**.

AUTHOR CONTRIBUTIONS

This paper was developed from the Master's thesis by FP. EB conceptualized idea for research, designed the project, and as project leader advised the FP, and assisted with field work. EB was also responsible for the research budget, data analysis and interpretation, and the writing, submission, and revision of the manuscript. PF was responsible for data collection, initial analysis, and interpretation and drafted some of the initial figures. Both authors performed critical revision of the manuscript for important intellectual content and approved the final manuscript.

FUNDING

This project was supported by grants to EB from the National Research Foundation of South Africa (Incentive Funding for Rated Researchers Programme) and the University of Cape Town Research Council as well as a Master's bursary to FP from BP Angola. The authors gratefully acknowledge their financial contributions. The funding bodies had no role in the design of the study and collection, analysis, and interpretation of data and in writing the manuscript. Opinions expressed and conclusions arrived at are those of the authors and are not necessarily to be attributed to the sponsors.

ACKNOWLEDGMENTS

Field assistants from EB's Sedimentology-Palaeontology Research Group at the University of Cape Town, particularly Mhairi Reid, Sanda Spelman, and Kenneth Chukwuma, are thanked for their help during several field trips. The authors acknowledge the warm reception, biostratigraphic guidance, and support in the field by the researchers of the Evolutionary Studies Institute at the University of the Witwatersrand, and in particular, they thank Michael Day, Sifelani Jirah, and Bruce Rubidge for the field guidance on the location of lower Beaufort Group biostratigraphic boundaries and the in-depth discussions on Karoo rocks, fossils, and life, past and present. The manuscript benefited greatly from the detailed, insightful, and constructive comments provided by Amanda Owen, Luca Colombera and several other anonymous reviewers. The authors sincerely appreciate their remarks and suggestions; however opinions expressed and conclusions arrived at are solely the authors' responsibility.

SUPPLEMENTARY MATERIAL

The Supplementary Material for this article can be found online at: https://www.frontiersin.org/articles/10.3389/feart.2020.521766/full#supplementary-material.

REFERENCES

Allen, J. P., Fielding, C. R., Gibling, M. R., and Rygel, M. C. (2002). Recognizing products of palaeoclimate fluctuation in the fluvial stratigraphic record: an example from the pennsylvanian to lower permian of Cape Breton Island, Nova Scotia. *Sedimentology* 61 (5), 1332–1381. doi:10.1111/j.1365-3091.2013.12102.x

Allen, J. R. L. (1983). Studies in fluviatile sedimentation: bars, bar-complexes and sandstone sheets (low-sinuosity braided streams) in the Brownstones (L. Devonian), Welsh Borders. *Sediment. Geol.* 33, 237–293. doi:10.1016/0037-0738(83)90076-3

Allen, J. R. L. (1970). Studies in fluviatile sedimentation; a comparison of fining-upwards cyclothems, with special reference to coarse-member composition and interpretation. *J. Sediment. Res.* 40, 298–323.

Allen, P. A. (2008). *Time scales of tectonic landscapes and their sediment routing systems*, 296. London, UK: Special Publication of the Geological Society of London, 7–28.

Blatt, H., Middleton, G. V., and Murray, R. C. (1972). *Origin of sedimentary rocks*. Englewood Cliffs, NJ: Prentice-Hall, 782 p.

Blewett, S. C. J., and Phillips, D. (2016). "An overview of Cape Fold Belt geochronology: implications for sediment provenance and the timing of orogenesis," in *Origin and evolution of the Cape mountains and Karoo Basin: geo-biohistory in a terrain with shale gas resources and need for conservationPart of the series regional geology reviews 8643*. Editors B. Linol and M. De Wit (Berlin, Germany: Springer-Verlag), 45–55. doi:10.1007/978-3-319-40859-0_5

Blewett, S. C. J., Phillips, D., and Matchan, E. L. (2019). Provenance of Cape Supergroup sediments and timing of Cape Fold belt orogenesis: constraints from high-precision 40Ar/39Ar dating of muscovite. *Gondwana Res.* 70, 201–221 doi:10.1016/j.gr.2019.01.009

Blum, M. D., and Törnqvist, T. E. (2000). Fluvial responses to climate and sea-level change: a review and look forward. *Sedimentology* 47, 2–48. doi:10.1046/j.1365-3091.2000.00008.x

Blum, M., Martin, J., Milliken, K., and Garvin, M. (2013). Paleovalley systems: insights from Quaternary analogs and experiments. *Earth Sci. Rev.* 116, 128–169. doi:10.1016/j.earscirev.2012.09.003

Bordy, E. M., Linkermann, S., and Prevec, R. (2011). Palaeoecological aspects of some invertebrate trace fossils from the mid-to upper permian Middleton formation (adelaide Subgroup, Beaufort group, Karoo Supergroup), eastern Cape, South Africa. *J. Afr. Earth Sci.* 61, 238–244. doi:10.1016/j.jafrearsci.2011.06.002

Bordy, E. M. (2018). SW Karoo study sites_Bordy & Paiva_End-Capitanian fluvial style. *Figshare. Dataset* doi:10.6084/m9.figshare.7217708.v1

Bryant, M., Falk, P., and Paola, C. (1995). Experimental study of avulsion frequency and rate of deposition. *Geology* 23, 365–368. doi:10.1130/0091-7613(1995)023<0365:ESOAFA>2.3.CO;2

Catuneanu, O. (2006). *Principles of sequence stratigraphy*. Amsterdam, Netherlands: Elsevier, 386.

Catuneanu, O. (2019). Model-independent sequence stratigraphy. *Earth Sci. Rev.* 188, 312–388. doi:10.1016/j.earscirev.2018.09.017

Catuneanu, O., Hancox, P. J., and Rubidge, B. S. (1998). Reciprocal flexural behaviour and contrasting stratigraphies: a new basin development model for the Karoo retroarc foreland system. *S. Afr.: Basin Res.* 10, 417–439. doi:10.1046/J.1365-2117.1998.00078.X

Catuneanu, O., Wopfner, H., Eriksson, P. G., Cairncross, B., Rubidge, B. S., Smith, R. M. H., et al. (2005). The Karoo basins of south-central Africa. *J. Afr. Earth Sci.* 43, 211–253. doi:10.1016/j.jafrearsci.2005.07.007

Catuneanu, O., and Bowker, D. (2001). Sequence stratigraphy of the Koonap and Middleton fluvial formations in the Karoo foredeep South Africa. *J. Afr. Earth Sci.* 33 (3), 579–595. doi:10.1016/S0899-5362(01)00095-1

Catuneanu, O., and Elango, H. N. (2001). Tectonic control on fluvial styles: the balfour formation of the Karoo Basin, South Africa. *Sediment. Geol.* 140, 291–313. doi:10.1016/S0037-0738(00)00190-1

Cole, D. I., Johnson, M. R., and Day, M. O. (2016). Lithostratigraphy of the Abrahamskraal Formation (Karoo Supergroup), South Africa. *S. Afr. J. Geol.* 119, 415–424. doi:10.2113/gssajg.119.2.415

Cole, D. I., and Wipplinger, P. E. (2001). *Sedimentology and molybdenum potential of the Beaufort group in the main Karoo Basin*. Pretoria, South Africa: Memoir of the Geological Survey, 225.

Colombera, L., Mountney, N. P., and McCaffrey, W. D. (2013). A quantitative approach to fluvial facies models: methods and example results. *Sedimentology* 60 (6), 1526–1558. doi:10.1111/sed.12050

Colombera, L., Mountney, N. P., and McCaffrey, W. D. (2015). A meta-study of relationships between fluvial channel-body stacking pattern and aggradation rate: implications for sequence stratigraphy. *Geology* 43, 283–286. doi:10.1130/G36385.1

Coney, L., Reimold, W. U., Hancox, P. J., Mader, D., Koeberl, C., McDonald, I., et al. (2007). Geochemical and mineralogical investigation of the Permian–Triassic boundary in the continental realm of the southern Karoo Basin, South Africa. *Palaeoworld*. 16, 67–104. doi:10.1016/j.palwor.2007.05.003

Dasgupta, P. (2002). Determination of paleocurrent direction from oblique sections of trough cross-stratification—a precise approach. *J. Sediment. Res.* 72, 217–219. doi:10.1306/050401720217

Day, M. O., Ramezani, J., Bowring, S. A., Sadler, P. M., Erwin, D. H., Abdala, F., et al. (2015). When and how did the terrestrial mid-Permian mass extinction occur? Evidence from the tetrapod record of the Karoo Basin, South Africa. *Proc. Biol. Sci.* 282 (1811), 20150834. doi:10.1098/rspb.2015.0834

Day, M. O., and Rubidge, B. S. (2014). A brief lithostratigraphic review of the Abrahamskraal and Koonap formations of the Beaufort Group, South Africa: towards a basin-wide stratigraphic scheme for the Middle Permian Karoo. *J. Afr. Earth Sci.* 100, 227–242. doi:10.1016/j.jafrearsci.2014.07.001

Day, M. O., and Rubidge, B. S. (2020). Biostratigraphy of the tapinocephalus assemblage zone (Beaufort group, Karoo Supergroup), South Africa. *S. Afr. J. Geol.* 123, 149–164. doi:10.25131/sajg.123.0014

Dickinson, W. R. (1970). Interpreting detrital modes of graywacke and arkose. *J. Sediment. Res.* 40, 695–707. doi:10.1306/74D72018-2B21-11D7-8648000102C1865D

Dickinson, W. R. (1985). "Interpreting provenance relations from detrital modes of sandstones," in *Provenance of arenites*. Editor G. Zuffa (Boston, MA: D. Reidel), 333–361.

Dingle, E. H., Sinclair, H. D., Attal, M., Milodowski, D. T., and Singh, V. (2016). Subsidence control on river morphology and grain size in the Ganga Plain. *Am. J. Sci.* 316 (8), 778–812. doi:10.2475/08.2016.03

Flood, Y. S., and Hampson, G. J. (2015). Quantitative analysis of the dimensions and distribution of channelized fluvial sandbodies within a large outcrop dataset: upper Cretaceous Blackhawk Formation. *J. Sediment. Res.* 85, 315–336. doi:10.2110/jsr.2015.25

Garzanti, E. (2016). From static to dynamic provenance analysis—sedimentary petrology upgraded. *Sediment. Geol.* 336, 3–13. doi:10.1016/j.sedgeo.2015.07.010

Garzanti, E. (2019). Petrographic classification of sand and sandstone. *Earth Sci. Rev.* 192, 545–563. doi:10.1016/j.earscirev.2018.12.014

Gibling, M. R. (2006). Width and thickness of fluvial channel bodies and valley fills in the geological record: a literature compilation and classification. *J. Sediment. Res.* 76, 731–770. doi:10.2110/jsr.2006.060

Gulliford, A. R., Flint, S. S., and Hodgson, D. M. (2014). Testing applicability of models of distributive fluvial systems or Trunk Rivers in ephemeral systems: reconstructing 3-D fluvial architecture in the Beaufort Group. *South Afr. J. Sed. Res.* 84 (12), 1147–1169. doi:10.2110/jsr.2014.88

Hampson, G. J., Jewell, T. O., Irfan, N., Gani, M. R., and Bracken, B. (2013). Modest changes in fluvial style with varying accommodation in regressive alluvial-to-coastal-plain wedge: Upper Cretaceous Blackhawk Formation, Wasatch Plateau, central Utah, U.S.A. *J. Sediment. Res.* 83, 145–169. doi:10.2110/jsr.2013.8

Hancox, P. J., and Rubidge, B. S. (2001). Breakthroughs in the biodiversity, biogeography, biostratigraphy, and basin analysis of the Beaufort Group. *J. Afr. Earth Sci.* 33, 563–577. doi:10.1016/S0899-5362(01)00081-1

Hansma, J., Tohver, E., Schrank, C., Jourdan, F., and Adams, D. (2015). The timing of the Cape Orogeny: New 40Ar/39Ar age constraints on deformation and cooling of the Cape Fold Belt, South Africa. *Gondwana Res.* 32, 122–137. doi:10.1016/j.gr.2015.02.005

Harms, J. C., Southard, J. B., and Walker, R. G. (1982). "Structures and Sequences in clastic rocks.–SEPM Short Course," in *Lecture notes* (Calgary, Canada: Society of Economic Paleontologists and Mineralogists (SEPM)), 9, 249 p.

Hartley, A. J., Weissmann, G. S., Nichols, G. J., and Warwick, G. L. (2010). Large distributive fluvial systems: Characteristics, distribution, and controls on development. *J. Sediment. Res.* 80 (2), 167–183. doi:10.2110/jsr.2010.016

High, L. R., and Picard, M. D. (1974). Reliability of cross-stratification types as paleocurrent indicators in fluvial rocks. *J. Sediment. Res.* 44, 158–168. doi:10.1306/74d729af-2b21-11d7-8648000102c1865d

Hirst, J. P. P. (1991). "Variations in alluvial architecture across the Oligo-Miocene Huesca fluvial system, Ebro Basin, Spain," in *Three-dimensional facies architecture of terrigenous clastic sediments and its implications for hydrocarbon discovery and recovery*. (Tulsa, Oklahoma: SEPM concepts in Sedimentology and paleontology). Editors A. D. Miall and N. Tyler, 3, 111–121. doi:10.2110/csp.91.03.0111

Holbrook, J., Scott, R. W., and Oboh-Ikuenobe, F. E. (2006). Base-level buffers and buttresses: a model for upstream versus downstream control on fluvial geometry and architecture within sequences. *J. Sediment. Res.* 76, 162–174. doi:10.2110/jsr.2005.10

Huang, Y., Chen, Z.-Q., Wignall, P. B., Grasby, S. E., Zhao, L., Wang, X., et al. (2018). Biotic responses to volatile volcanism and environmental stresses over the Guadalupian-Lopingian (Permian) transition. *Geology* 47, 175–178. doi:10.1130/G45283.1

Ingersoll, R. V., Bullard, T. F., Ford, R. L., Grimm, J. P., Pickle, J. D., and Sares, S. W. (1984). The Effect of grain size on detrital modes: a test of the Gazzi-Dickinson point-counting method. *J. Sediment. Res.* 54, 103–116. doi:10.1306/212F878D-2B24-11D7-8648000102C1865D

Johnson, M. R., Van Vuuren, C. J., Hegenberger, W. F., Key, R., and Show, U. (1996). Stratigraphy of the Karoo Supergroup in southern Africa: an overview. *J. Afr. Earth Sci.* 23 (2), 3–15. doi:10.1016/S0899-5362(96)00048-6

Johnson, M. R., Van Vuuren, C. J., Visser, J. N. J., Cole, D. I., Wickens, H. D., Christie, A. D. M., et al. (2006). "Sedimentary rocks of the Karoo Supergroup," in *The geology of South Africa*. Editor M.R. Johnson, et al. (Pretoria, South Africa: Geological Society of South Africa and Council for Geoscience), 461–499.

Johnson, M. R., and Wolmarans, L. (2008). *Simplified geological map of the republic of South Africa and kingdoms of Lesotho and Swaziland*. Pretoria, South Africa: Council for Geoscience.

Keyser, A. W., and Smith, R. M. H. (1978). Vertebrate biozonation of the Beaufort Group with special reference to the western Karoo Basin. *Ann. Geol. Surv. South Afr.* 12, 1–36.

Keyser, A. W. (1966). Some indications of arid climate during the deposition of the Beaufort Series. *Ann. Geol. Surv. South Afr.* 5, 77–79.

Kraus, M. J. (1999). Paleosols in clastic sedimentary rocks: their geologic applications. *Earth Sci. Rev.* 47, 41–70.

Lanci, L., Tohver, E., Wilson, A., and Flint, S. (2013). Upper Permian magnetic stratigraphy of the lower Beaufort Group, Karoo Basin. *Earth Planet Sci. Lett.* 375, 123–134. doi:10.1016/j.epsl.2013.05.017

Leeder, M. R. (1993). Tectonic controls upon drainage basin development, river channel migration and alluvial architecture: implications for hydrocarbon reservoir development and characterization. *Spec. Publ. Geol. Soc. Lond.* 73, 7–22. doi:10.1144/GSL.SP.1993.073.01.02

Long, D. G. F. (2006). Architecture of pre-vegetation sandy-braided perennial and ephemeral river deposits in the Paleoproterozoic Athabasca Group, northern Saskatchewan, Canada as indicators of Precambrian fluvial style. *Sediment. Geol.* 190, 71–95. doi:10.1016/j.sedgeo.2006.05.006

Loock, J. C., Brynard, H. J., Heard, R. G., Kitching, J. W., and Rubidge, B. S. (1994). The stratigraphy of the lower Beaufort Group in an area north of Laingsburg, South Africa. *J. Afr. Earth Sci.* 18, 185–195. doi:10.1016/0899-5362(94)90003-5

Lucas, S. G. (2017). Permian tetrapod extinction events. *Earth Sci. Rev.* 170, 31–60. doi:10.1016/j.earscirev.2017.04.008

Mackey, S. D., and Bridge, J. S. (1995). Three-dimensional model of alluvial stratigraphy; theory and applications. *J. Sediment. Res.* 65, 7–31. doi:10.1306/D42681D5-2B26-11D7-8648000102C1865D

Miall, A. D. (2010). "Alluvial deposits," in *Facies models four*. Editors N. P. James and R. W. Dalrymple (Calgary: Geological Association of Canada), 105–137.

Miall, A. D. (1988). Architectural elements and bounding surfaces in fluvial deposits: anatomy of the Kayenta Formation (Lower Jurassic). Southwest Colorado. *Sediment. Geol.* 55, 233–262. doi:10.1016/0037-0738(88)90133-9

Miall, A. D. (1985). Architectural-element analysis: a new method of facies analysis applied to fluvial deposits. *Earth Sci. Rev.* 22, 261–308. doi:10.1016/0012-8252(85)90001-7

Miall, A. D. (2013). *Fluvial depositional systems*. New York, NY: Springer, 316.

Miall, A. D. (1974). Paleocurrent analysis of alluvial sediments; a discussion of directional variance and vector magnitude. *J. Sediment. Res.* 44, 1174–1185.

Miall, A. D. (2016). *Stratigraphy: a modern synthesis*. Berlin, Germany: Springer-Verlag, 454.

Miall, A. D. (1978). Tectonic setting and syndepositional deformation of molasse and other nonmarine-paralic sedimentary basins. *Can. J. Earth Sci.* 15 (10), 1613–1632. doi:10.1139/e78-166

Miall, A. D. (2017). "The contribution of fluvial sedimentology to petroleum exploration and the science of stratigraphy", in Proceedings of the 11th International Conference on Fluvial Sedimentology. 22–23, Calgary, Canada, July 17-21, 2017. [Abstract].

Miall, A. D. (2014). The emptiness of the stratigraphic record: a preliminary evaluation of the missing time in the Mesaverde Group, Book Cliffs, Utah. *J. Sediment. Res.* 84, 457–469. doi:10.2110/jsr.2014.40

Miall, A. D. (1996). *The geology of fluvial deposits: sedimentary facies, basin analysis, and petroleum geology*. Berlin, Germany: Springer-Verlag, 582.

Miall, A. D. (2015). "Updating uniformitarianism: stratigraphy as just a set of 'frozen accidents'," in *Strata and time: probing the gaps in our understanding*. Editors D. G. Smith, R. J. Bailey, P. M. Burgess, and A. J. Fraser (London, UK: Special Publication of the Geological Society of London), 404, 11–36.

Moscariello, A. (2018). Alluvial fans and fluvial fans at the margins of continental sedimentary basins: geomorphic and sedimentological distinction for geo-energy exploration and development, 440. (London, UK: Special Publication of the Geological Society of London), 215–243.

North, C. P., and Davidson, S. K. (2012). Unconfined alluvial flow processes: recognition and interpretation of their deposits, and the significance for palaeogeographic reconstruction. *Earth Sci. Rev.* 111, 199–223. doi:10.1016/j.earscirev.2011.11.008

Owen, A., Nichols, G. J., Hartley, A. J., Weissmann, G. S., and Scuderi, L. A. (2015). Quantification of a distributive fluvial system: the Salt Wash DFS of the Morrison Formation, SW USA. *J. Sediment. Res.* 85, 544–561.

Owen, A., Ebinghaus, A., Hartley, A. J., Santos, M. G., and Weissmann, G. S. (2017a). Multi-scale classification of fluvial architecture: An example from the Palaeocene–Eocene Bighorn Basin, Wyoming. *Sedimentology* 64, 1572–1596. doi:10.1111/sed.12364

Owen, A., Nichols, G. J., Hartley, A. J., and Weissmann, G. S. (2017b). Vertical trends within the prograding Salt Wash distributive fluvial system, SW United States. *Basin Res.* 29, 64–80.

Owen, A., Hartley, A. J., Ebinghaus, A., Weissmann, G. S., and Santos, M. G. (2019). Basin-scale predictive models of alluvial architecture: Constraints from the Palaeocene–Eocene, Bighorn Basin, Wyoming, USA. *Sedimentology* 66, 736–763.

Paiva, F. (2016). Fluvial facies architecture and provenance history of the Abrahamskraal-Teekloof Formation transition (Lower Beaufort Group) in the main Karoo Basin. MSc dissertation. Cape Town (South Africa): University of Cape Town. Open access; Digitally published and archived here: http://hdl.handle.net/11427/20615.

Parrish, J. T. (1998). *Interpreting pre-quaternary climate from the geologic record*. New York, NY: Columbia University Press.

Payenberg, T., Willis, B., Bracken, B., Posamentier, H. W., Pyrcz, M., Pusca, V., et al. (2011). Revisiting the subsurface classification of fluvial sandbodies. in *Search and discovery article*. Houston, TX: American Association of Petroleum Geologists, Annual Convention and Exhibition. 90124.

Pimentel, N. L., Wright, V. P., and Azevedo, T. M. (1996). Distinguishing early groundwater alteration effects from pedogenesis in ancient alluvial basins: examples from the Paleogene of southern Portugal. *Sediment. Geol.* 105, 1–10. doi:10.1016/0037-0738(96)00034-6

Retallack, G. J. (2005). Pedogenic carbonate proxies for amount and seasonality of precipitation in paleosols. *Geology* 33, 333–336. doi:10.1130/G21263.1

Rey, K., Amiot, R., Fourel, F., Rigaudier, T., Abdala, F., Day, M. O., et al. (2016). Global climate perturbations during the Permo-Triassic mass extinctions recorded by continental tetrapods from South Africa. *Gondwana Res.* 37, 384–396. doi:10.1016/j.gr.2015.09.008

Rubidge, B. S., Erwin, D. H., Ramezani, J., Bowring, S. A., and de Klerk, W. J. (2013). High-precision temporal calibration of Late Permian vertebrate biostratigraphy: U-Pb zircon constraints from the Karoo Supergroup. *S. Afr. J. Geol.* 41 (3), 363–366. doi:10.1130/G33622.1

Rubidge, B. S., Hancox, P. J., and Catuneanu, O. (2000). Sequence analysis of the Ecca-Beaufort contact in the southern Karoo of South Africa. *S. Afr. J. Geol.* 103 (1), 81–96. doi:10.2113/103.1.81

Rubidge, B. S. (2005). Re-uniting lost continents: Fossil reptiles from the ancient Karoo and their wanderlust. *S. Afr. J. Geol.* 108, 135–172.

Shanley, K. W., and McCabe, P. J. (1994). Perspectives on the Sequence Stratigraphy of Continental Strata. *AAPG (Am. Assoc. Pet. Geol.) Bull.* 78, 544–568. doi:10.1306/bdff9258-1718-11d7-8645000102c1865d

Sheldon, N. D. (2005). Do red beds indicate paleoclimatic conditions? A Permian case study. *Palaeogeogr. Palaeoclimatol. Palaeoecol.* 228, 305–319. doi:10.1016/j.palaeo.2005.06.009

Shellnutt, J. G., Denyszyn, S. W., and Mundil, R. (2012). Precise age determination of mafic and felsic intrusive rocks from the Permian Emeishan large igneous province (SW China). *Gondwana Res.* 22 (1), 118–126. doi:10.1016/j.gr.2011.10.009

Shukla, U. K., Singh, I. B., Sharma, M., and Sharma, S. (2001). A model of alluvial megafan sedimentation: Ganga Megafan. *Sediment. Geol.* 144, 243–262. doi:10.1016/S0037-0738(01)00060-4

Singh, H., Parkash, B., and Gohain, K. (1993). Facies analysis of the Kosi megafan deposits. *Sediment. Geol.* 85, 87–113. doi:10.1016/0037-0738(93)90077-I

Sinha, R., Ahmad, J., Gaurav, K., and Morin, G. (2014). Shallow subsurface stratigraphy and alluvial architecture of the Kosi and Gandak megafans in the Himalayan foreland basin, India. *Sediment. Geol.* 301, 133–149. doi:10.1016/j.sedgeo.2013.06.008

Slate, J. L., Smith, G. A., Wang, Y., and Cerling, T. E. (1996). Carbonate-paleosol genesis in the PlioPleistocene St. Davis Formation, Southeastern Arizona. *J. Sediment. Res.* 66, 85–94.

Smith, R. M. H. (1990). Alluvial paleosols and pedofacies sequences in the Permian Lower Beaufort of the southwestern Karoo Basin, South Africa. *J. Sediment. Petrol.* 60, 258–276. doi:10.1306/212F916A-2B24-11D7-8648000102C1865D

Smith, R. M. H. (1987). Morphology and depositional history of exhumed Permian point bars in the southwestern Karoo South Africa. *J. Sediment. Petrol.* 57, 19–29. doi:10.1306/212F8A8F-2B24-11D7-8648000102C1865D

Smith, R. M. H. (1993). Sedimentology and ichnology of floodplain paleosurfaces in the Beaufort Group (Late Permian), Karoo Sequence, South Africa. *Palaios* 8, 339–357. doi:10.2307/3515265

Smith, R. M. H. (1979). The sedimentology and taphonomy of floodplain deposits of the Lower Beaufort (Adelaide Subgroup) strata near Beaufort West, Cape Province. *Ann. Geo. Sur. South Afr.* 12, 37–68.

Srivastava, P., Rajak, M. K., Sinha, R., Pal, D. K., and Bhattacharyya, T. (2010). A high-resolution micromorphological record of the Late Quaternary paleosols

from Ganga–Yamuna interfluve: stratigraphic and paleoclimatic implications. *Quat. Int.* 227, 127–142. doi:10.1016/J.QUAINT.2010.02.019

Stear, W. M. (1980). Channel sandstone and bar morphology of the Beaufort Group uranium district near Beaufort West. *Trans. Geol. Soc. S. Afr.* 83, 391–398.

Stear, W. M. (1985). Comparison of the bedform distribution and dynamics of modern and ancient sandy ephemeral flood deposits in the southwestern Karoo region. *Sediment. Geol.* 45, 209–230. doi:10.1016/0037-0738(85)90003-X

Stear, W. M. (1983). Morphological characteristics of ephemeral stream channel and overbank splay sandstone bodies in the Permian Lower Beaufort Group, Karoo Basin, South Africa, 6. Karoo Basin, South Africa: International Association of Sedimentologists Special Publication, 405–420.

Stear, W. M. (1978). Sedimentary structures related to fluctuating hydrodynamic conditions in flood-plain deposits of the Beaufort Group near Beaufort West, Cape. *Trans. Geol. Soc. S. Afr.* 74, 111–131.

Tandon, S. K., Sinha, R., Gibling, M. R., Dasgupta, A. S., and Ghazanfari, P. (2008). Late Quaternary evolution of the Ganga Plains: myths and misconceptions, recent developments and future directions, 66. Bangalore, India: Memoir of the Geological Society of India, 259–299.

Tankard, A., Welsink, H., Aukes, P., Newton, R., and Stettler, E. (2012). "Geodynamic interpretation of the Cape and Karoo basins, South Africa," in *Regional geology and tectonics: phanerozoic passive margins, cratonic basins and global tectonic maps*. Editors D. G. Roberts and A. W. Bally (Amsterdam, Netherlands: Elsevier), 869–945.

Viglietti, P. A., Smith, R. M. H., Angielczyk, K. D., Kammerer, C. F., Fröbisch, J., and Rubidge, B. S. (2016). The Daptocephalus Assemblage Zone (Lopingian), South Africa: a proposed biostratigraphy based on a new compilation of stratigraphic ranges. *J. Afr. Earth Sci.* 113, 153–164. doi:10.1016/j.jafrearsci.2015.10.011

Walker, T. R. (1976). "Diagenetic origin of continental red beds," in *The continental permian in central, west, and south europe*. Editor H. Faulke (Dordrecht, Netherlands: Riedel Publishing), 171, 240–282.

Wang, J., and Plink-Bjorklund, P. (2019). Stratigraphic complexity in fluvial fans: Lower Eocene Green River Formation, Uinta Basin, USA. *Basin Res.* 31, 892–919. doi:10.1111/bre.12350

Weissmann, G. S., Hartley, A. J., Scuderi, L. A., Nichols, G. J., Davidson, S. K., Owen, A., et al. (2013). "Prograding distributive fluvial systems: geomorphic models and ancient examples," in *New Frontiers in paleopedology and terrestrial paleoclimatology SEPM* (London, UK: Special Publication), 104, 131–147.

Weissmann, G. S., Hartley, A. J., Scuderi, L. A., Nichols, G. J., Owen, A., Wright, S., et al. (2015). Fluvial geomorphic elements in modern sedimentary basins and their potential preservation in the rock record: a review. *Geomorphology* 250, 187–219. doi:10.1016/j.geomorph.2015.09.005

Weltje, G. J., and von Eynatten, H. (2004). Quantitative provenance analysis of sediments: an introduction. *Sediment. Geol.* 171 (1), 1–11. doi:10.1016/j.sedgeo.2004.05.007

Wilson, A., Flint, S., Payenberg, T., Tohver, E., and Lanci, L. (2014). Architectural styles and sedimentology of the fluvial lower Beaufort Group, Karoo Basin, South Africa. *J. Sediment. Res.* 84 (4), 326–348. doi:10.2110/jsr.2014.28

Wizevich, M. C. (1992). "Photomosaics of outcrops: useful photographic techniques," in *The three-dimensional facies architecture of terrigenous clastic sediments and its implications for hydrocarbon discovery and recovery SEPM concepts in Sedimentology and paleontology*. Editors A. D. Miall and N. Tyler, (Tulsa, OK: Society for Sedimentary Geology) 3, 22–24.

Wright, V. P., and Marriott, S. B. (2007). The dangers of taking mud for granted: lessons from Lower Old Red Sandstone dryland river systems of South Wales. *Sediment. Geol.* 195, 91–100. doi:10.1016/j.sedgeo.2006.03.028

Wright, V. P., and Marriott, S. B. (1993). The sequence stratigraphy of fluvial depositional systems: the role of floodplain sediment storage. *Sediment. Geol.* 86, 203–210. doi:10.1016/0037-0738(93)90022-W

Zecchin, M., and Catuneanu, O. (2013). High-resolution sequence stratigraphy of clastic shelves I: units and bounding surfaces. *Mar. Petrol. Geol.* 39, 1–25. doi:10.1016/j.marpetgeo.2012.08.015

Zhang, B., Yao, S., Wignall, P. B., Hu, W., Liu, B., and Ren, Y. (2019). New timing and geochemical constraints on the Capitanian (Middle Permian) extinction and environmental changes in deep-water settings: Evidence from the Lower Yangtze region of South China. *J. Geol. Soc.* 176, 588–608. doi:10.1144/jgs2018-137

Zhou, M. F., Malpas, J., Song, X. Y., Robinson, P. T., Sun, M., Kennedy, A. K., et al. (2002). A temporal link between the Emeishan large igneous province (SW China) and the end-Guadalupian mass extinction. *Earth Planet Sci. Lett.* 196, 113–122. doi:10.1016/S0012-821X(01)00608-2

Conflict of Interest: The authors declare that the research was conducted in the absence of any commercial or financial relationships that could be construed as a potential conflict of interest.